ARTICLE

Luminescent copper(I) complexes with bisphosphane and halogen-substituted 2,2'-bipyridine ligands

Sarah Keller,[a] Alessandro Prescimone,[a] Henk Bolink,[b] Michele Sessolo,[b] Giulia Longo,[b] Laura Martínez-Sarti,[b] José M. Junquera-Hernández,[b] Edwin C. Constable,[a] Enrique Ortí*[b] and Catherine E. Housecroft*[a]

Heteroleptic [Cu(P^P)(N^N)][PF$_6$] complexes, where N^N is a halo-substituted 2,2'-bipyridine (bpy) and P^P is either bis(2-(diphenylphosphino)phenyl)ether (POP) or 4,5-bis(diphenylphosphino)-9,9-dimethylxanthene (xantphos) have been synthesized and investigated. To stabilize the tetrahedral geometry of the copper(I) complexes, the steric demands of the bpy ligands have been increased by introducing 6- or 6,6'-halo-substituents in 6,6'-dichloro-2,2'-bipyridine (6,6'-Cl$_2$bpy), 6-bromo-2,2'-bipyridine (6-Brbpy) and 6,6'-dibromo-2,2'-bipyridine (6,6'-Br$_2$bpy). The solid-state structures of [Cu(POP)(6,6'-Cl$_2$bpy)][PF$_6$], [Cu(xantphos)(6,6'-Cl$_2$bpy)][PF$_6$]·CH$_2$Cl$_2$, [Cu(POP)(6-Brbpy)][PF$_6$] and [Cu(xantphos)(6-Brbpy)][PF$_6$]·0.7Et$_2$O obtained from single crystal X-ray diffraction are described including the pressure dependence of the structure of [Cu(POP)(6-Brbpy)][PF$_6$]. The copper(I) complexes with either POP or xantphos and 6,6'-Cl$_2$bpy, 6-Brbpy and 6,6'-Br$_2$bpy are orange-to-red emitters in solution and yellow-to-orange emitters in the solid state, and their electrochemical and photophysical properties have been evaluated with the help of density functional theory (DFT) calculations. The emission properties are strongly influenced by the substitution pattern that largely affects the geometry of the emitting triplet state. [Cu(POP)(6,6'-Cl$_2$bpy)][PF$_6$] and [Cu(xantphos)(6,6'-Cl$_2$bpy)][PF$_6$] show photoluminescence quantum yields of 15 and 17%, respectively, in the solid state, and these compounds were tested as luminophores in light-emitting electrochemical cells (LECs). The devices exhibit orange electroluminescence and very short turn-on times (<5 to 12 s). Maximum luminance values of 121 and 259 cd m^{-2} for [Cu(POP)(6,6'-Cl$_2$bpy)][PF$_6$] and [Cu(xantphos)(6,6'-Cl$_2$bpy)][PF$_6$], respectively, were achieved at an average current density of 100 A m^{-2}; external quantum efficiencies of 1.2% were recorded for both complexes.
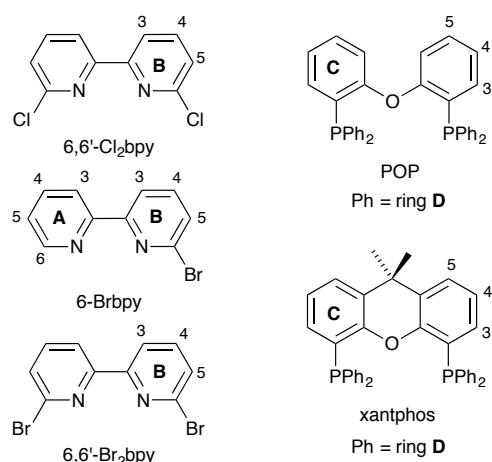
Introduction

The development of light-emitting electrochemical cells (LECs) with ionic transition-metal complexes (iTMCs) as emitters initially used ruthenium(II) complexes based on [Ru(bpy)$_3$]$^{2+}$ (bpy = 2,2'-bipyridine) in the emissive layer.[1,2] A much broader spectrum of emission colours is achieved by using cyclometallated iridium(III) complexes of the type [Ir(C^N)$_2$(N^N)]$^+$, the archetype complex being [Ir(ppy)$_2$(bpy)]$^+$ (Hppy = 2-phenylpyridine).[3] While LECs and OLEDs (organic light-emitting diodes) based on Ir-iTMCs remain an active area of research, attention has recently turned to the use of Cu-iTMCs.[3,4,5] In contrast to ruthenium and iridium, copper is Earth-abundant and thus leads to low-cost LECs. McMillin first demonstrated the potential of copper(I)-based emitters,[6,7] and the most studied families for LECs are [Cu(POP)(N^N)]$^+$ and [Cu(xantphos)(N^N)]$^+$ complexes (POP = bis(2-(diphenylphosphino)phenyl)ether, xantphos = 4,5-bis(diphenylphosphino)-9,9-dimethylxanthene and N^N is usually a derivative of bpy or phen)).[8,9,10,11,12,13,14,15,16]

In [Cu(POP)(N^N)]$^+$ and [C(xantphos)(N^N)]$^+$, the emission properties of the Cu-iTMC can be altered by introducing substituents into the 6- and 6'-positions of bpy or the 2- and 9-positions of phen.[6,9,10] Significant enhancement of LEC performance is observed with the introduction of simple alkyl groups (methyl or ethyl) at these positions.[10] Monomeric copper(I) complexes with halido ligands coordinating the copper atom, as well as dimeric complexes with bridging halido ligands between the copper atoms, show good emissive properties, largely because they exhibit thermally activated delayed fluorescence (TADF), and are promising materials for light-emitting devices.[17,18,19,20,21,22] We have previously investigated the effects of introducing peripheral halo-substituents into [Cu(P^P)(6,6'-Me$_2$-4,4'-Ph$_2$bpy)][PF$_6$] complexes and found that fluorine and chlorine substitution

leads to improved properties of the complexes and the respective LECs.[16] However, the number of copper(I) complexes in the literature containing a halo-substituted N^N chelating ligand is surprisingly few. The homoleptic [Cu(6,6'-Br$_2$bpy)$_2$][ClO$_4$][23] and heteroleptic [Cu(6,6'-Br$_2$bpy)(bpy(Mes)$_2$)][BF$_4$][24] complexes are two examples with a halo-substituted bpy. Most of the reported compounds contain halo-functionalized phenanthrolines,[25,26,27] with [Cu(5-Cl-phen)(PPh$_3$)$_2$]$^+$ and [Cu(4,7-Cl$_2$-phen)(PPh$_3$)$_2$]$^+$ being two examples.[28]

We now explore the effects on the [Cu(P^P)(bpy)][PF$_6$] complexes of introducing chloro- and bromo-substituents into the bpy domain using 6- or 6,6'-substitution patterns on the [Cu(P^P)(bpy)][PF$_6$] complexes. We were interested in determining whether stabilization of the copper(I) tetrahedral geometry brought about by introducing halo-groups into the 6-position of the bpy unit would be beneficial in terms of enhanced photophysical properties and LEC performance compared to the use of alkyl groups.[9,10] Alkyl groups are weakly electron donating (+I), and halogen atoms can have a positive inductive effect on the *ortho* and *para* positions of a π system (the so-called +I_π effect) in combination with a +M effect.[29] We argued that these two combined effects should have an influence on the orbital characteristics of the complex, the HOMO–LUMO gap and, therefore, the colour of the emission.

Scheme 1. Structures of ligands with ring and atom labels for NMR spectroscopic assignments.

Experimental

General

^{1}H, ^{13}C and ^{31}P NMR spectra were recorded at room temperature using a Bruker Avance III-500 or III-400 NMR spectrometer. ^{1}H and ^{13}C NMR chemical shifts were referenced to residual solvent peaks with respect to δ(TMS) = 0 ppm, and ^{31}P NMR chemical shifts with respect to δ(85% aqueous H$_3$PO$_4$) = 0 ppm. Solution absorption and emission spectra were measured using an Agilent 8453 spectrophotometer and a Shimadzu RF-5301PC spectrofluorometer, respectively.

Electrospray ionization (ESI) mass spectra were recorded on a Bruker esquire 3000plus or Shimadzu LCMS-2020 instrument. Photoluminescence quantum yields (PLQYs) for CH$_2$Cl$_2$ solution and powder samples were measured using a Hamamatsu absolute photoluminescence (PL) quantum yield spectrometer C11347 Quantaurus-QY. The system performs absolute measurements and does not require known reference standards. Emission lifetimes and powder emission spectra were measured with a Hamamatsu Compact Fluorescence lifetime Spectrometer C11367 Quantaurus-Tau, using an LED light source with λ_{exc} = 365 nm. Low temperature photoluminescence spectra and lifetime were obtained using an LP920-KS instrument from Edinburgh Instruments. 410 nm excitation was obtained from pulsed third-harmonic radiation from a Quantel Brilliant b Nd:YAG laser equipped with a Rainbow optical parameter oscillator (OPO). The laser pulse duration was ~10 ns and the pulse frequency 10 Hz, with a typical pulse energy of 7 mJ. Detection of the spectra occurred on an iCCD camera from Andor. Single-wavelength kinetics were recorded using a photomultiplier tube.

PLQY for thin films was measured on quartz substrates and the complexes were deposited by spin-coating using the same solutions employed in the preparation of the devices. The PLQY was measured with a Hamamatsu C9920 absolute quantum yield spectrometer. The system performs absolute measurements and does not require known reference standards. The low temperature setup consists in an integrating sphere with a double walled quartz dewar filled with liquid nitrogen. Compounds were dissolved at room temperature in 2-methyltetrahydrofuran (Me-THF) and the solutions were transferred into quartz cuvettes. The cuvettes were immersed in the liquid nitrogen and the PLQY was measured at low temperature.

The compounds 6,6'-dichloro-2,2'-bipyridine (6,6'-Cl$_2$bpy)[30] and [Cu(MeCN)$_4$][PF$_6$][31] were prepared using literature methods and the NMR spectroscopic data of 6,6'-Cl$_2$bpy matched those reported. POP was purchased from Acros, xantphos from Fluorochem, 6-bromo-2,2'-bipyridine (6-Brbpy) and 6,6'-dibromo-2,2'-bipyridine (6,6'-Br$_2$bpy) from TCI chemicals. All chemicals were used as received.

[Cu(POP)(6,6'-Cl$_2$bpy)][PF$_6$]. A colourless solution of [Cu(MeCN)$_4$][PF$_6$] (93 mg, 0.25 mmol) and POP (134 mg, 0.25 mmol) in CH$_2$Cl$_2$ (40 mL) was stirred for 2 h. Then 6,6'-Cl$_2$bpy (56 mg, 0.25 mmol) was added and the yellow solution was stirred for another 2 h. The solution was filtered and the solvent from the filtrate was removed in vacuo. The orange powder was redissolved in CH$_2$Cl$_2$ and layered with Et$_2$O. This gave [Cu(POP)(6,6'-Cl$_2$bpy)][PF$_6$] as orange crystals (208 mg, 0.21 mmol, 86%). ^{1}H NMR (500 MHz, CD$_2$Cl$_2$) δ/ppm 8.10 (dd, J = 7.9 Hz, 2H, H^{B3}), 7.98 (d, J = 7.9 Hz, 2H, H^{B4}), 7.41 (d, J = 7.9 Hz, 2H, H^{B5}), 7.32–7.25 (m, 6H, H^{C5+D4}), 7.16–7.08 (m, 20H, H$^{C3+C4+D2+D3}$), 6.86 (m, 2H, H^{C6}). ^{13}C NMR (126 MHz, CD$_2$Cl$_2$) δ/ppm 158.6 (s, C^{C1}), 152.6 (s, C^{B2}), 152.1 (s, C^{B6}), 141.8 (s, C^{B4}), 134.2 (s, C^{C3}), 133.7 (t, J = 8.5 Hz, C^{D2}), 132.6 (s, C^{C5}), 131.8 (t, J = 17.5 Hz, C^{D1}), 130.4 (s, C^{D4}), 129.1 (t, J = 5.3 Hz, C^{D3}), 127.7 (s, C^{B5}), 125.9 (t, J = 16.2 Hz, C^{C2}), 125.4

(s, C^{C4}), 121.9 (s, C^{B3}), 120.1 (s, C^{C6}). ^{31}P NMR (162 MHz, CD_2Cl_2) δ/ppm −12.3 (broad, FWHM = 180 Hz, POP), −144.5 (septet, J_{PF} = 710 Hz, $[PF_6]^-$). ESI MS: m/z 827.0 $[M–PF_6]^+$ (base peak, calc. 827.1). Found C 57.59, H 4.21, N 3.13; $C_{46}H_{34}Cl_2CuF_6N_2OP_3$ requires C 56.83, H 3.53, N 2.88%.

[Cu(xantphos)(6,6'-Cl$_2$bpy)][PF$_6$]. A colourless solution of xantphos (145 mg, 0.25 mmol) and 6,6'-Cl$_2$bpy (56 mg, 0.25 mmol) in CH_2Cl_2 (20 mL) was added dropwise to a colourless solution of $[Cu(MeCN)_4][PF_6]$ (93 mg, 0.25 mmol) in CH_2Cl_2 (20 mL). After stirring for 2h, the yellow solution was filtered and the solvent was removed in vacuo. The orange-yellow powder was redissolved in CH_2Cl_2 and layered with Et$_2$O. This gave [Cu(xantphos)(6,6'-Cl$_2$bpy)][PF$_6$] as yellow crystals in good yield (202 mg, 0.20 mmol, 80%). ^{1}H NMR (500 MHz, $(CD_3)_2CO$) δ/ppm 8.36 (d, J = 7.5 Hz, 2H, H^{B3}), 8.17 (t, J = 7.9 Hz, 2H, H^{B4}), 7.81 (dd, J = 7.8, 1.4 Hz, 2H, H^{C5}), 7.66 (d, J = 7.7 Hz, 2H, H^{B5}), 7.43–7.40 (m, 4H, H^{D4}), 7.29 (t, J = 7.7 Hz, 2H, H^{C4}), 7.25–7.20 (m, 16H, H^{D2+D3}), 7.00 (m, 2H, H^{C3}), 1.73 (s, 6H, H$^{xantphos-Me}$). ^{13}C NMR (126 MHz, $(CD_3)_2CO$) δ/ppm 156.0 (C^{C1}), 151.5 (C^{B2}), 142.7 (C^{B4}), 134.1 (t, J = 7.9 Hz, C^{D2}), 132.3 (t, J = 16.9 Hz, C^{D1}), 131.2 (C^{C3}), 131.0 (C^{D4}), 129.7 (t, J = 4.9 Hz, C^{D3}), 128.6 (C^{C5}), 128.0 (m, C^{C4+C2}), 122.7 (C^{B3}), 36.7 (C$^{xantphos-bridge}$), 29.0 (C$^{xantphos-Me}$). ^{31}P NMR (162 MHz, CD_2Cl_2) δ/ppm −11.9 (broad, FWHM = 150 Hz, xantphos), −144.5 (septet, J_{PF} = 710 Hz, $[PF_6]^-$). ESI MS: m/z 867.0 $[M–PF_6]^+$ (base peak, calc. 867.1). Found C 57.64, H 4.22, N 3.12; $C_{49}H_{38}Cl_2CuF_6N_2OP_3$ requires C 58.14, H 3.78, N 2.77%.

[Cu(POP)(6-Brbpy)][PF$_6$]. A colourless solution of $[Cu(MeCN)_4][PF_6]$ (93 mg, 0.25 mmol) and POP (134 mg, 0.25 mmol) in CH_2Cl_2 (40 mL) was stirred for 2 h. Then 6-Brbpy (59 mg, 0.25 mmol) was added and the yellow solution was stirred for another 2 h. The solution was filtered and the solvent was removed in vacuo. [Cu(POP)(6-Brbpy)][PF$_6$] was isolated as a yellow powder (226 mg, 0.23 mmol, 92%). ^{1}H NMR (500 MHz, CD_2Cl_2) δ/ppm 8.20 (d, J = 7.8 Hz, 2H, H^{A3+B3}), 8.01–7.98 (m, 1H, H^{A6}), 7.92 (td, J = 8.0, 1.6 Hz, 1H, H^{A4}), 7.83 (t, J = 7.9 Hz, 1H, H^{B4}), 7.52 (dd, J = 7.9, 0.6 Hz, 1H, H^{B5}), 7.49–7.46 (m, 4H, H$^{D2/D2'}$), 7.37 (t, J = 7.5 Hz, 2H, H$^{D4/D4'}$), 7.27 (t, J = 7.3 Hz, 4H, H$^{D3/D3'}$), 7.26–7.23 (m, 4H, H$^{C5+ D4/D4'}$), 7.08 (t, J = 7.8 Hz, 4H, H$^{D3/D3'}$), 7.03 (td, J = 7.7, 0.8 Hz, 2H, H^{C4}), 7.00 (m, 1H, H^{A5}), 6.95 (dtd, J = 8.2, 2.5, 1.0 Hz, 2H, H^{C6}), 6.90 (dtd, J = 7.8, 4.1, 1.6 Hz, 2H, H^{C3}), 6.80–6.76 (m, 4H, H$^{D2/D2'}$). ^{13}C NMR (126 MHz, CD_2Cl_2) δ/ppm 158.3 (t, J = 6.1 Hz, C^{C1}), 153.7 (C^{B2}), 151.4 (t, J = 2.3 Hz, C^{A2}), 149.6 (C^{A6}), 143.1 (C^{B6}), 141.0 (C^{B4}), 139.0 (C^{A4}), 135.1 (t, J = 8.5 Hz, C$^{D2/D2'}$), 134.6 (C^{C3}), 132.7 (t, J = 7.7 Hz, C$^{D2/D2'}$), 132.6 (C$^{C5+ D4/D4'}$), 131.5 (t, J = 18.1 Hz, C$^{D1/D1'}$), 131.1 (C$^{D4/D4'}$), 130.8 (C^{B5}), 130.6 (t, J = 16.2 Hz, C$^{D1/D1'}$), 129.3 (t, J = 5.2 Hz, C$^{D3/D3'}$), 129.1 (t, J = 4.9 Hz, C$^{D3/D3'}$), 126.5 (C^{A5}), 125.7 (t, J = 2.5 Hz, C^{C4}), 125.0 (t, J = 15.1 Hz, C^{C2}), 123.1 (C^{A3}), 121.7 (C^{B3}), 120.6 (t, J = 2.1 Hz, C^{C6}). ^{31}P NMR (162 MHz, CD_2Cl_2) δ/ppm −11.2 (broad, FWHM = 250 Hz, POP), −144.5 (septet, J_{PF} = 710 Hz, $[PF_6]^-$). ESI MS: m/z 837.4 $[M–PF_6]^+$ (base peak, calc. 837.1). Found C 55.99, H 3.77, N 3.06; $C_{46}H_{35}BrCuF_6N_2OP_3$ requires C 56.25, H 3.59, N 2.85%.

[Cu(xantphos)(6-Brbpy)][PF$_6$]. A colourless solution of xantphos (145 mg, 0.25 mmol, 1.0 eq) and 6-Brbpy (59 mg, 0.25 mmol, 1.0 eq) in CH_2Cl_2 (20 mL) was added to a colourless solution of $[Cu(MeCN)_4][PF_6]$ (93 mg, 0.25 mmol, 1.0 eq) in CH_2Cl_2 (20 mL) and the resulting yellow solution was stirred for 2 h. The solvent was removed in vacuo and the yellow powder was redissolved in CH_2Cl_2 and layered with Et$_2$O. This gave [Cu(xantphos)(6-Brbpy)][PF$_6$] as yellow crystals in good yield (244 mg, 0.24 mmol, 96 %). ^{1}H NMR (500 MHz, $(CD_3)_2CO$, 298 K) δ/ppm 8.56 (dd, J = 8.0, 0.5 Hz, 1H, H^{B3}), 8.50 (d, J = 8.2 Hz, 1H, H^{A3}), 8.38 (d, J = 4.3 Hz, 1H, H^{A6}), 8.15 (t, J = 7.9 Hz, 1H, H^{B4}), 8.12 (td, J = 7.8, 1.5 Hz, 1H, H^{A4}), 7.87 (dd, J = 7.9, 0.6 Hz, 1H, H^{B5}), 7.84 (dd, J = 7.8, 1.4 Hz, 2H, H^{C4}), 7.51 (ddd, J = 7.5, 5.1, 0.9 Hz, 1H, H^{A5}), 7.42 (t, J = 7.4 Hz, 2H, H$^{D4/D4'}$), 7.34 (t, J = 7.4 Hz, 2H, H$^{D4/D4'}$), 7.29 (m, 6H, H$^{C5+D3/D3'}$), 7.22–7.15 (m, 8H, H$^{D2/D2'+D3/D3'}$), 7.08–7.04 (m, 4H, H$^{D2/D2'}$), 6.78–6.74 (m, 2H, H^{C3}), 1.84 (s, 3H, H$^{xantphos-Me}$), 1.70 (s, 3H, H$^{xantphos-Me}$). ^{13}C NMR (126 MHz, $(CD_3)_2CO$, 298 K) δ/ppm 155.9 (C^{C1}), 153.9 (C^{B2}), 152.0 (C^{A2}), 149.8 (C^{A6}), 143.1 (C^{B6}), 142.2 (C^{B4}), 140.1 (C^{A4}), 134.6 (C^{C6}), 133.8 (t, J = 8.1 Hz, C$^{D2/D2'}$), 133.7 (t, J = 8.1 Hz, C$^{D2/D2'}$), 132.6 (C$^{D1/D1'}$), 132.3 (C$^{D1/D1'}$), 131.7 (C^{C3}), 131.5 (C^{B5}), 131.1 (C$^{D4/D4'}$), 130.9 (C$^{D4/D4'}$), 129.9 (t, J = 4.9 Hz, C$^{D3/D3'}$), 129.7 (t, J = 4.9 Hz, C$^{D3/D3'}$), 128.6 (C^{C4}), 127.6 (C^{A5}), 126.1 (t, J = 2.7 Hz, C^{C5}), 124.3 (C^{A3}), 122.6 (C^{B3}), 121.4 (t, J = 14.4 Hz, C^{C2}), 36.8 (C$^{xantphos-bridge}$), 30.1 (C$^{xantphos-Me}$), 27.3 (C$^{xantphos-Me}$). ^{31}P{^{1}H} NMR (202 MHz, $(CD_3)_2CO$, 298 K) δ/ppm −12.4 (broad, FWHM = 350 Hz, xantphos), −144.2 (septet, J_{PF} = 709 Hz, $[PF_6]^-$). ESI MS: m/z 877.3 $[M–PF_6]^+$ (base peak, calc. 877.1). Found C 57.50, H 4.03, N 3.05; $C_{49}H_{39}BrCuF_6N_2OP_3$ requires C 57.57, H 3.85, N 2.74%.

[Cu(POP)(6,6'-Br$_2$bpy)][PF$_6$]. A colourless solution of $[Cu(MeCN)_4][PF_6]$ (56 mg, 0.15 mmol) and POP (81 mg, 0.15 mmol) in CH_2Cl_2 (40 mL) was stirred for 2 h. Then 6,6'-Br$_2$bpy (47 mg, 0.15 mmol) was added and the yellow solution was stirred for another 2 h. The solution was filtered and the solvent from the filtrate was removed in vacuo. [Cu(POP)(6,6'-Br$_2$bpy)][PF$_6$] was isolated as an orange-yellow powder in good yield (93 mg, 0.09 mmol, 60 %). ^{1}H NMR (500 MHz, $(CD_3)_2CO$, 298 K) δ/ppm 8.44 (dd, J = 8.0, 0.8 Hz, 2H, H^{B3}), 8.08 (t, J = 7.9 Hz, 2H, H^{B4}), 7.83 (dd, J = 7.9, 0.6 Hz, 2H, H^{B5}), 7.44 (ddd, J = 8.2, 7.1, 2.0 Hz, 2H, H^{C5}), 7.37–7.33 (m, 4H, H^{D4}), 7.30–7.20 (m, 20H, H$^{D2+D3+C3+C4}$), 7.05–7.02 (m, 2H, HC^{C6}). ^{13}C NMR (126 MHz, $(CD_3)_2CO$, 298 K) δ/ppm 159.0 (t, J = 5.7 Hz, C^{C1}), 153.9 (C^{B2}), 143.2 (C^{B6}), 142.1 (C^{B4}), 134.6 (C^{C3}), 134.2 (t, J = 7.7 Hz, C^{D2}), 133.1 (C^{C5}), 132.6 (t, J = 17.2 Hz, C^{D1}), 132.2 (C^{B5}), 130.8 (C^{D4}), 129.5 (t, J = 4.6 Hz, C^{D3}), 126.3 (C^{C2}), 125.9 (t, J = 2.3 Hz, C^{C4}), 123.0 (C^{B3}), 120.7 (t, J = 1.8 Hz, C^{C6}). ^{31}P NMR (162 MHz, $(CD_3)_2CO$, 300 K) δ/ppm −13.6 (broad, FWHM = 155 Hz, POP), −144.2 (septet, J_{PF} = 707 Hz, $[PF_6]^-$). ESI MS: m/z 915.1 $[M–PF_6]^+$ (base peak, calc. 915.0). Found C 51.78, H 3.43, N 3.13; $C_{46}H_{34}Br_2CuF_6N_2OP_3$ requires C 52.07, H 3.23, N 2.64%.

[Cu(xantphos)(6,6'-Br$_2$bpy)][PF$_6$]. A colourless solution of xantphos (145 mg, 0.25 mmol, 1.0 eq) and 6,6-Br$_2$bpy (78 mg, 0.25 mmol, 1.0 eq) in CH_2Cl_2 (20 mL) was added to a

colourless solution of $[Cu(MeCN)_4][PF_6]$ (93 mg, 0.25 mmol, 1.0 eq) in CH_2Cl_2 (20 mL) and the resulting yellow solution was stirred for 2 h. The solvent was removed in vacuo and the yellow powder was redissolved in CH_2Cl_2 and layered with Et_2O. $[Cu(xantphos)(6,6'-Br_2bpy)][PF_6]$ was isolated as a canary-yellow powder in excellent yield (260 mg, 0.24 mmol, 96 %). ^1H NMR (500 MHz, $(CD_3)_2CO$, 298 K) δ/ppm 8.31 (dd, J = 8.0, 0.8 Hz, 2H, H^{B3}), 8.03 (t, J = 7.9 Hz, 2H, H^{B4}), 7.80 (dd, J = 7.9, 0.8 Hz, 2H, H^{B5}), 7.79 (dd, J = 7.8, 1.4 Hz, 2H, H^{C5}), 7.43 (t, J = 7.3 Hz, 4H, H^{D4}), 7.33–7.29 (m, 8H, H^{D2}), 7.29 (d, J = 5.1 Hz, 2H, H^{C4}), 7.25 (t, J = 7.6 Hz, 8H, H^{D3}), 7.10–7.06 (m, 2H, H^{C3}), 1.71 (s, 6H, $H^{xantphos-Me}$). ^{13}C NMR (126 MHz, $(CD_3)_2CO$, 298 K) δ/ppm 155.9 (t, J = 6.4 Hz, C^{C1}), 153.4 (C^{B2}), 142.5 (C^{B6}), 142.1 (C^{B4}), 134.3 (t, J = 7.6 Hz, C^{D2}), 134.2 (t, J = 1.9 Hz, C^{C6}), 132.1 (t, J = 16.9 Hz, C^{D1}), 131.9 (C^{B5}), 131.2 (C^{C3}), 131.0 (C^{D4}), 129.6 (t, J = 4.6 Hz, C^{D3}), 128.6 (C^{C5}), 126.0 (t, J = 2.4 Hz, C^{C4}), 123.0 (C^{B3}), 36.7 ($C^{xantphos-bridge}$), 29.0 ($C^{xantphos-Me}$). ^{31}P NMR (162 MHz, $(CD_3)_2CO$, 300 K) δ/ppm −13.0 (broad, FWHM = 140 Hz, xantphos), −144.2 (septet, J_{PF} = 708 Hz, $[PF_6]^-$). ESI MS: m/z 955.2 $[M–PF_6]^+$ (base peak, calc. 955.0). Found C 53.38, H 3.92, N 2.63; $C_{49}H_{38}Br_2CuF_6N_2OP_3$ requires C 53.45, H 3.48, N 2.54%.

Crystallography

Ambient pressure data were collected on a Bruker Kappa Apex2 diffractometer with data reduction, solution and refinement using the programs APEX[32] and CRYSTALS.[33] For $[Cu(xantphos)(6,6'-Cl_2bpy)][PF_6]·CH_2Cl_2$, SQUEEZE[34] was used to treat the solvent region. 92 e^-/unit cell were found: that corresponds to 46 e^-/formula. This can be rationalised as one molecule of CH_2Cl_2 per formula unit; the formulae have been appropriately modified.

Structural analysis was carried out using Mercury v. 3.7.[35,36] High-pressure single crystal experiments were carried out using a Merrill-Bassett diamond anvil cell[37] (half-opening angle 40°), equipped with Boehler-Almax diamonds with 600 μm culets and a tungsten gasket.[38] Hexane was used as hydrostatic medium and a small ruby chip was loaded into the cell as the pressure calibrant with the ruby fluorescence used to measure the pressure.[39] Diffraction data were collected using synchrotron radiation of wavelength λ = 0.4859 Å at room temperature on a Newport IS4CCD (4 circle) diffractometer with a Pilatus 300K detector at Station I19 at the Diamond Light Source, Harwell Science and Innovation Campus. Integrations were carried out using the program CrysAlisPro[40] and absorption corrections with the program ABSPACK.[40] Refinements were carried out with CRYSTALS using the ambient pressure structure as starting model; the ambient model was used to refine the structure at 0.16 GPa, then the model at 0.16 GPa was used to refine the structure at 1.30 GPa, and so on.

[Cu(POP)(6,6'-Cl₂bpy)][PF₆]. $C_{46}H_{34}Cl_2CuF_6N_2OP_3$, M = 972.15, light orange block, monoclinic, space group $P2_1/c$, a = 10.4351(6), b = 18.8158(10), c = 22.3310(12) Å, β = 99.434(4)°, U = 4325.3(4) Å^3, Z = 4, D_c = 1.493 Mg m^{-3},

μ(Cu-Kα) = 3.457 mm^{-1}, T = 123 K. Total 48007 reflections, 7953 unique, R_{int} = 0.067. Refinement of 4914 reflections (673 parameters) with $I > 2\sigma(I)$ converged at final R_1 = 0.0642 (R_1 all data = 0.0990), wR_2 = 0.1610 (wR_2 all data = 0.1949), gof = 0.9366. CCDC 1535144.

[Cu(xantphos)(6,6'-Cl₂bpy)][PF₆]·CH₂Cl₂. $C_{50}H_{40}Cl_4CuF_6N_2OP_3$, M = 1012.21, yellow block, triclinic, space group $P-1$, a = 11.2546(11), b = 14.3360(13), c = 18.0998(16) Å, α = 113.273(4), β = 100.571(4), γ = 90.543(4)°, U = 2626.3(4) Å^3, Z = 2, D_c = 1.39 Mg m^{-3}, μ(Cu-Kα) = 3.825 mm^{-1}, T = 123 K. Total 32725 reflections, 9421 unique, R_{int} = 0.038. Refinement of 9049 reflections (883 parameters) with $I > 2\sigma(I)$ converged at final R_1 = 0.1077 (R_1 all data = 0.1098), wR_2 = 0.2742 (wR_2 all data = 0.2745), gof = 0.9428. CCDC 1535142.

[Cu(POP)(6-Brbpy)][PF₆]. $C_{46}H_{35}BrCuF_6N_2OP_3$, M = 982.16, yellow block, monoclinic, space group $P2_1/c$, a = 15.3402(6), b = 14.2344(5), c = 19.2659(7) Å, β = 90.9159(12)°, U = 4206.34(15) Å^3, Z = 4, D_c = 1.551 Mg m^{-3}, μ(Cu-Kα) = 3.491 mm^{-1}, T = 123 K. Total 35307 reflections, 7329 unique, R_{int} = 0.022. Refinement of 7293 reflections (541 parameters) with $I > 2\sigma(I)$ converged at final R_1 = 0.0281 (R_1 all data = 0.0282), wR_2 = 0.0673 (wR_2 all data = 0.0673), gof = 0.8936. CCDC 1535141. For high pressure data and respective CCDC codes of this structure see Table S1†.

[Cu(xantphos)(6-Brbpy)][PF₆]·0.7Et₂O. $C_{49}H_{39}BrCuF_6N_2OP_3·0.7C_4H_{10}O$ or $C_{51.80}H_{46}BrCuF_6N_2O_{1.70}P_3$, M = 1074.11, yellow block, triclinic, space group $P-1$, a = 11.0101(5), b = 15.0994(7), c = 18.1016(9) Å, α = 108.840(3), β = 98.138(3), γ = 109.910(3)°, U = 2568.6(2) Å^3, Z = 2, D_c = 1.389 Mg m^{-3}, μ(Cu-Kα) = 2.916 mm^{-1}, T = 123 K. Total 32455 reflections, 9339 unique, R_{int} = 0.035. Refinement of 8428 reflections (596 parameters) with $I > 2\sigma(I)$ converged at final R_1 = 0.1060 (R_1 all data = 0.1121), wR_2 = 0.2611 (wR_2 all data = 0.2626), gof = 1.0223. CCDC 1583875.

Computational details

Density functional theory (DFT) calculations were performed for the $[Cu(P^\wedge P)(N^\wedge N)]^+$ cations ((P^P) = POP and xantphos; (N^N) = bpy, 6,6'-Cl₂bpy, 6-Brbpy and 6,6'-Br₂bpy) using the A.03 revision of the Gaussian 16 program package.[41] The Becke's three-parameter B3LYP exchange-correlation functional[42,43] was used together with the "double-ζ" quality def2svp basis set for C, H, Br, Cl, N and O atoms and the "triple-ζ" quality def2tzpv basis set for Cu atoms.[44,45] The D3 Grimme's dispersion term with Becke-Johnson damping was added to the B3LYP functional (B3LYP-D3) to get a better description of the intramolecular non-covalent interactions.[46,47] These interactions are expected to play a relevant role in determining the molecular geometry of the studied complexes owing to the presence of the bulky POP and xantphos ligands. The geometries of all the complexes in both their singlet ground electronic state (S_0) and their lowest-energy triplet excited state (T_1) were optimized without imposing any symmetry restriction. For T_1 the spin unrestricted UB3LYP approximation was used, with a spin multiplicity of three. The lowest-lying

excited states of each complex, both singlets and triplets, were computed at the minimum-energy geometry optimized for S_0 using the time-dependent DFT (TD-DFT) approach.[48,49,50] TD-DFT B3LYP calculations were performed both using the def2svp2+def3tzpv basis set, explained above, and the 6-31G** basis set for non-copper atoms[51] plus the "double-ζ" quality LANL2DZ basis set for the Cu atom.[52] The 6-31G**+LANL2DZ basis set leads to absorption and emission energies in good accord with experimental results, whereas the results obtained with the def2svp2+def3tzpv basis set largely underestimate the experimental energies and are not discussed. The S_1 and T_1 states were also optimized using the TD-DFT approach and the 6-31G**+LANL2DZ and def2svp2+def3tzpv basis sets to obtain a better estimate of the adiabatic energy difference separating the minima of these two states. All the calculations were performed in the presence of the solvent (CH_2Cl_2). Solvent effects were considered within the self-consistent reaction field (SCRF) theory using the polarized continuum model (PCM) approach.[53,54,55]

LEC fabrication

LECs were prepared on top of patterned indium tin oxide (ITO, 15 Ω $\square^{-1}$) coated glass substrates previously cleaned as follows: (a) 5 min sonication with soap solution, (b) 5 min sonication in deionized water, (c) 5 min sonication in isopropanol and (d) UV-O_3 lamp for 20 min. Prior to the deposition of the emitting layer, a layer of poly(3,4-ethylenedioxythiophene): poly(styrenesulfonate) (PEDOT:PSS) (CLEVIOS^{TM} P VP AI 4083, Heraeus) was spin-coated on the glass substrate at 1000 rpm, and then annealed at 150 ºC for 15 min. The as- prepared PEDOT:PSS had a thickness of 60 nm, measured with an Ambios XP-1 profilometer. The active layer solution was prepared by dissolving the copper complex and the ionic liquid 1-ethyl-3-methylimidazolium hexafluoridophosphate [Emim][PF$_6$] (>98.5%, Sigma-Aldrich) in butan-2-one in a molar ratio of 4:1. The solutions were filtered through 0.25 μm pore filters and immediately spin-coated on the substrate at 1500 rpm for 60 s, resulting in a 110 nm thick emitting layer. The devices were then transferred to an inert atmosphere glovebox (<0.1 ppm O_2 and H_2O), where a layer of aluminium (100 nm, the top electrode) was thermally evaporated onto the devices using an Edwards Auto500 evaporator integrated in the glovebox. The active area of each pixel in the devices was 6.5 mm^2. The devices were not encapsulated and were characterized inside the glovebox at room temperature. The same solutions employed in the preparation of the devices were also deposited on quartz substrates and used for the evaluation of the photoluminescence quantum yield with a Hamamatsu absolute quantum yield C9920. The device lifetime was measured by applying a pulsed current (block wave at 1 kHz frequency with a 50% duty cycle) while monitoring the voltage and luminance versus time by a True Colour Sensor MAZeT (MTCSiCT Sensor) with a Botest OLT OLED Lifetime-Test System. The average current density is determined by multiplying the peak current density by the time-on time and dividing by the duty cycle. The average luminance is directly

obtained as the average from a photodiode and calibrated with a luminance meter. The electroluminescent (EL) spectra were measured using an Avantes AvaSpec-2048 Fiber Optic Spectrometer during device lifetime measurement.

Results and discussion

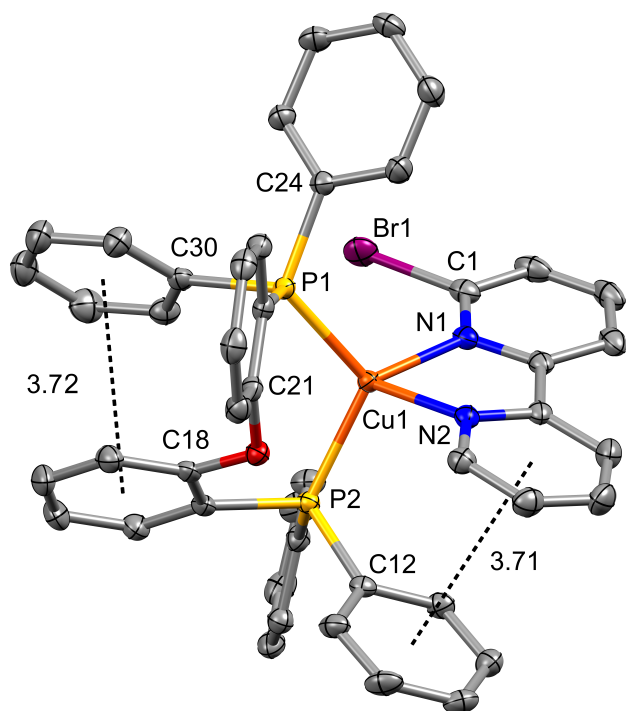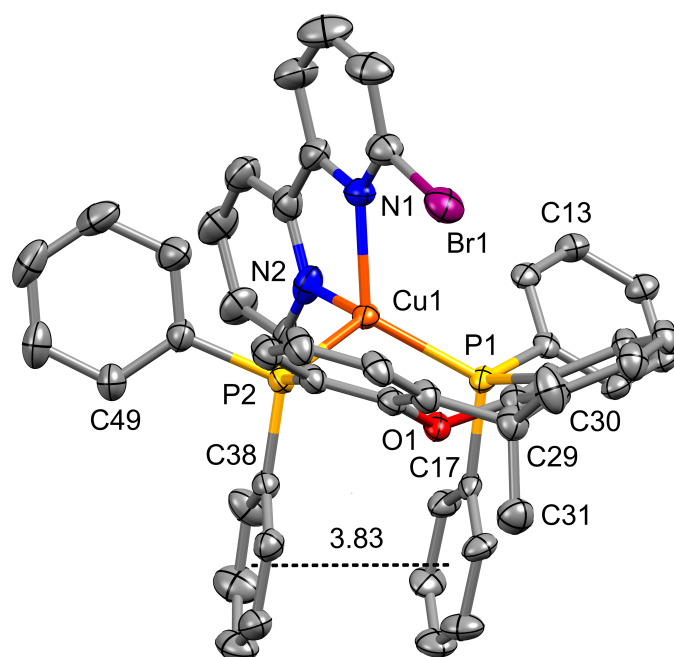### Synthesis and characterization of [Cu(P^P)(N^N)][PF$_6$] complexes

The [Cu(P^P)(N^N)][PF$_6$] complexes were synthesized by addition of the ligands to a solution of [Cu(MeCN)$_4$][PF$_6$] in CH_2Cl_2. For the complexes with POP, the synthetic procedure used the established sequential addition of the two ligands; the bpy ligand was added after stirring POP and [Cu(MeCN)$_4$][PF$_6$] for two hours.[56] Simultaneous addition of the two ligands was used for the preparation of [Cu(xantphos)(N^N)][PF$_6$]. The compounds [Cu(POP/xantphos)(N^N)][PF$_6$] with N^N = 6,6'-Cl$_2$bpy, 6-Brbpy or 6,6'-Br$_2$bpy were isolated as yellow or orange solids in yields of 60 to 96%. All compounds were characterized by mass spectrometry, elemental analysis, and multinuclear NMR spectroscopies using 2D methods to assign the spectra. Details are given in the Experimental Section.

Structural characterization

X-ray quality crystals of [Cu(POP)(6,6'-Cl$_2$bpy)][PF$_6$], [Cu(xantphos)(6,6'-Cl$_2$bpy)][PF$_6$]·CH_2Cl_2, [Cu(POP)(6-Brbpy)][PF$_6$] and [Cu(xantphos)(6-Brbpy)][PF$_6$]·0.7Et$_2$O were obtained by diffusion of Et$_2$O into CH_2Cl_2 solutions of the respective compound. The structures of the cations are illustrated in Fig. 1–2 and Fig. S1†–S2† and important angles and bond distances are summarized in Table 1. The compounds [Cu(xantphos)(6,6'-Cl$_2$bpy)][PF$_6$]·CH_2Cl_2 and [Cu(xantphos)(6-Brbpy)][PF$_6$]·0.7Et$_2$O crystallize in the triclinic space group $P-1$, whereas [Cu(POP)(6,6'-Cl$_2$bpy)][PF$_6$] and [Cu(POP)(6-Brbpy)][PF$_6$] both crystallize in the monoclinic space group $P2_1/c$. In [Cu(POP)(6,6'-Cl$_2$bpy)][PF$_6$] (Fig. S1†) and [Cu(xantphos)(6,6'-Cl$_2$bpy)][PF$_6$]·CH_2Cl_2 (Fig. S2†), the POP and xantphos ligands are each disordered over two sites, each with 50% occupancy.

Table 1. Comparison of structural parameters of the [Cu(P^P)(N^N)][PF$_6$] complexes.

Complex cation	Cu–P distance / Å	Cu–N distance / Å	P–Cu–P chelating angle / deg	N–Cu–N chelating angle / deg	Angle between CuP$_2$ and CuN$_2$ planes / deg	N–C–C–N torsion angle /deg
[Cu(POP)(6,6'-Cl$_2$bpy)]$^+$	Cu1–P1 = 2.2422(13); Cu1–P2 = 2.2751(14)	Cu1–N1 = 2.134(4); Cu1–N2 = 2.107(4)	117.19(5)	78.15(17)	86.0	15.8(11)
[Cu(xantphos)(6,6'-Cl$_2$bpy)]$^+$	Cu1–P1 = 2.2545(15); Cu1–P2 = 2.2875(15)	Cu1–N1 = 2.097(5); Cu1–N2 = 2.104(5)	114.74(6)	76.7(2)	89.5	0.7(20)
[Cu(POP)(6-Brbpy)]$^+$	Cu1–P1 = 2.2362(5); Cu1–P2 = 2.2628(5)	Cu1–N1 = 2.0858(14); Cu1–N2 = 2.0782(14)	114.280(18)	79.53(6)	82.0	9.5(4)
[Cu(xantphos)(6-Brbpy)]$^+$	Cu1–P1 = 2.2428(15); Cu1–P2 = 2.2615(17)	Cu1–N1 = 2.087(5); Cu1–N2 = 2.050(3)	113.90(6)	81.7(2)	87.0	0.8(16)

Fig. 1 Structure of the cation [Cu(POP)(6-Brbpy)]$^+$ in [Cu(POP)(6-Brbpy)][PF$_6$]. Ellipsoids plotted at 50% probability level, H atoms omitted, centroid···centroid distances = 3.71 and 3.72 Å, respectively.

Fig. 2 Structure of the cation [Cu(xantphos)(6-Brbpy)]$^+$ in [Cu(xantphos)(6-Brbpy)][PF$_6$]·0.7Et$_2$O. Ellipsoids plotted at 50% probability level, H atoms omitted, centroid···centroid distance = 3.83 Å.

In each of the four complexes, the copper(I) centre exhibits a distorted tetrahedral geometry, with the angles between the planes containing the CuN$_2$ and CuP$_2$ units lying in the range 82.0 to 89.5°. For the cations with xantphos, the angles between these planes are close to the 90° of an ideal tetrahedral coordination geometry (89.5° for [Cu(xantphos)(6,6'-Cl$_2$bpy)]$^+$ and 87.0° for [Cu(xantphos)(6-Brbpy)]$^+$). These are also the cations in which the bpy ligand is twisted the least, with N–C–C–N torsions of ≈1°. The Cu–P and Cu–N bond distances as well as the N–Cu–N and P–Cu–P chelating angles are unexceptional for all the complexes (Table 1).

In the structure of [Cu(POP)(6-Brbpy)][PF$_6$] (Fig. 1), there are two π-stacking interactions with parameters within the range described by Janiak.[57] The ring of the POP backbone that includes C18 and the phenyl ring that includes C30 have a centroid···centroid distance of 3.72 Å; the angle between the ring planes is 13.7°, making this a non-optimal interaction. The second π-stacking contact is between the rings containing C12 and N2 (Fig. 1) with a centroid···centroid distance of 3.71 Å and inter-plane angle of 9.8°. The Cu1···Br1 distance is 3.5017(3) Å, indicating little or no interaction between these atoms. In the [Cu(xantphos)(6-Brbpy)]$^+$ cation (Fig. 2), the phenyl rings with C17 and C38 exhibit a π-stacking interaction with a centroid···centroid distance of 3.83 Å and an angle between the ring planes of 7.0°.

The single crystal X-ray structure of [Cu(POP)(6-Brbpy)][PF$_6$] was also investigated under conditions of increasing pressure (0.16, 1.3, 1.8, 3.5, 4.2 and 4.5 GPa) in the hydrostatic environment of a diamond pressure cell and the overlaid structures of the [Cu(POP)(6-Brbpy)]$^+$ cations are

illustrated in Fig. S3†. With increased pressure, the cell lengths *a*, *b* and *c* and the angle *β* decrease and the volume shrinks from 4274(3) Å^3 at 0.16 GPa to 3450.3(19) Å^3 at 4.5 GPa, which is around 81% of the original volume. The structure remained in the monoclinic space group $P2_1/c$ with $Z = 4$. Angles and bond lengths of the cation (see caption to Fig. S3†) undergo only minor changes, confirming the rigidity of its geometry.

Electrochemistry

The electrochemical behaviour of the heteroleptic complexes was investigated using cyclic voltammetry (CV) and the oxidation potentials $E_{1/2}^{ox}$ are summarized in Table 2. The oxidation potentials for the copper(I) complexes with halo-substituted bpy ligands are shifted to higher potentials (+0.90 to +0.98 V) compared to complexes with unmodified bpy (+0.72 V for [Cu(POP)(bpy)][PF$_6$] and +0.76 V for [Cu(xantphos)(bpy)][PF$_6$][58]). The higher potentials required for the Cu$^+$/Cu^{2+} oxidation for the halo-substituted complexes are consistent with the electron-withdrawing effects of the halogens. The oxidation processes are quasi-reversible and no reduction process was visible for any of the complexes. In general, substituents in the 6- or 6,6'-positions should stabilize a tetrahedral geometry leading to a higher Cu$^+$/Cu^{2+} oxidation potential, and this is in agreement with the data in Table 2. Compared to the analogous alkyl-substituted complexes [Cu(POP)(6-Mebpy)][PF$_6$][9] (+0.69 V) and [Cu(POP)(6,6'-Me$_2$bpy)][BF$_4$] (+0.82 V),[59] higher oxidation potentials are observed for the halo-substituted complexes owing to the electron-withdrawing effect of the halo-groups on the coordinating nitrogen atoms. Halogen atoms next to the nitrogen in the bpy unit therefore have the combined effect of stabilizing the tetrahedral geometry and decreasing the electron density at the nitrogen donor.

Table 2 Cyclic voltammetry data for [Cu(P^P)(bpy)][PF$_6$] complexes referenced to internal Fc/Fc$^+$ = 0.0 V; CH$_2$Cl$_2$ (freshly distilled) solutions with [^{n}Bu$_4$N][PF$_6$] as supporting electrolyte and scan rate of 0.1 V s^{-1}. Processes are quasi-reversible.

Complex cation	$E_{1/2}^{ox}$ / V	$(E_{pc} - E_{pa}$ / mV)
[Cu(POP)(bpy)]$^+$	+0.72^a	110
[Cu(xantphos)(bpy)]$^+$	+0.76^a	110
[Cu(POP)(6,6'-Cl$_2$bpy)]$^+$	+0.98	170
[Cu(xantphos)(6,6'-Cl$_2$bpy)]$^+$	+0.93	90
[Cu(POP)(6-Brbpy)]$^+$	+0.93	90
[Cu(xantphos)(6-Brbpy)]$^+$	+0.90	90
[Cu(POP)(6,6'-Br$_2$bpy)]$^+$	+0.97	120
[Cu(xantphos)(6,6'-Br$_2$bpy)]$^+$	+0.98	140

^{a}Data from reference 58.

DFT calculations: Optimized geometries and molecular orbitals

The geometries of all the [Cu(P^P)(N^N)]$^+$ cations, including the [Cu(POP)(bpy)]$^+$ and [Cu(xantphos)(bpy)]$^+$ non-substituted complexes, in their electronic ground state (S$_0$) were optimized at the DFT B3LYP-D3/(def2svp+def2tzvp) level in the presence of the solvent (CH$_2$Cl$_2$) and without imposing any symmetry restriction (see the Experimental section for full computational details). The results obtained for the most representative geometrical parameters of the Cu(I) coordination sphere are summarized in Table S2†. Calculations correctly reproduce the distorted tetrahedral structures observed experimentally for [Cu(POP)(6,6'-Cl$_2$bpy)]$^+$ and [Cu(POP)(6-Brbpy)]$^+$. Compared to the values from single crystal X-ray diffraction, the Cu−P and Cu−N bond distances are predicted with an accuracy of 0.04 Å and the P−Cu−P and N−Cu−N chelating angles of 4º. In the optimized geometries, the angle defined by the P−Cu−P and N−Cu−N planes, which exemplifies the deviation from the orthogonal disposition of the P^P and N^N ligands, has values of 77.3, 79.3 and 81.5º for [Cu(POP)(6,6'-Cl$_2$bpy)]$^+$, [Cu(POP)(6-Brbpy)]$^+$ and [Cu(POP)(6,6'-Cl$_2$bpy)]$^+$, respectively, underestimating the X-ray values for [Cu(POP)(6,6'-Cl$_2$bpy)]$^+$ (86.0º) and [Cu(POP)(6-Brbpy)]$^+$ (82.0º). Theoretical calculations also overestimate the torsion angle of the bpy ligand by about 6º (compare Table 1 and S2†). The differences between theoretical and X-ray geometries are largely due to the fact that the former are obtained for an isolated molecule optimized in solution and do not take into account the packing forces acting in the solid state. The intermolecular forces reduce the coordination distances and the torsion angles and increase the chelating angles.

For the xantphos-containing complexes, two minimum-energy structures were found for [Cu(xantphos)(6-Brbpy)]$^+$ with a very small energy difference of ≈0.60 kcal mol^{-1} between them (Fig. S4†). One of these structures closely resembles that obtained from X-ray diffraction, featuring the π-stacking between the phenyl ring attached to P1 and containing C17 and the one attached to P2 and containing C38, with a centroid⋯centroid distance of 3.80 Å; this is in good agreement with the experimental value (3.83 Å, Fig. 2). In the second structure with a slightly lower energy, this stacking does not occur and instead, there is π-stacking between the phenyl ring attached to P1 and including C13 and the ring of the pyridine including N2, with a centroid⋯centroid distance of 3.84 Å. The existence of the two minima and their relative energy ordering was also reproduced in the gas-phase. However, only the lower energy structure was converged for [Cu(xantphos)(6,6'-Cl$_2$bpy)]$^+$ and [Cu(xantphos)(6,6'-Br$_2$bpy)]$^+$ showing centroid⋯centroid distances of 3.63 and 3.64 Å, respectively.

The geometry of the first triplet excited state (T$_1$) was also optimized at the UB3LYP level for all the [Cu(P^P)(N^N)]$^+$ cations, and the most significant geometry parameters are also summarized in Table S2†. The molecular geometry in the T$_1$ state significantly differs from that in the ground state S$_0$. As explained below, the T$_1$ state implies a charge transfer from a *d* orbital of the Cu atom to a molecular orbital centered on the bpy ligand. The metal atom is therefore partially oxidized and tends to adopt the square-planar coordination sphere commonly found for four-fold coordinated d^9 Cu(II) complexes, rather than the tetrahedral coordination exhibited in the ground state and typical of d^{10} Cu(I) coordination complexes. This trend is easily verified by the angle formed by the N−Cu−N and P−Cu−P planes, which decreases on going from S$_0$ to T$_1$ as the molecule becomes more planar (Table S2†). For the reference

complexes [Cu(POP)(bpy)]$^+$ and [Cu(xantphos)(bpy)]$^+$, bearing no substituent on the bpy ligand, this angle changes from 80.4 and 86.9° in S_0 to 59.7 and 57.5° in T_1, respectively, showing a reduction of almost 30° for [Cu(xantphos)(bpy)]$^+$. When halogen atoms are introduced in the 6,6'-positions of the bpy ligand, a smaller angle reduction is obtained in passing from S_0 to T_1 because the substituents impede the movement of the ligand towards a more planar disposition of the cation geometry. The angle reduction is of only 7–9° in the case of the disubstituted [Cu(P^P)(6,6'-Cl$_2$bpy)]$^+$ and [Cu(P^P)(6,6'-Br$_2$bpy)]$^+$ complexes, and increases to 11.1 and 19.4° for the less-impeded mono-substituted [Cu(POP)(6-Brbpy)]$^+$ and [Cu(xantphos)(6-Brbpy)]$^+$ complexes, respectively. These trends are in good accord with those previously reported for similar complexes bearing CF$_3$ or CH$_3$ groups in 6,6'-positions of the bpy ligand.[58] Therefore, the distortion from the tetrahedral structure on going from S_0 to T_1 is limited by the number and size of substituents in the 6,6'-positions.

Fig. 3 shows the energies and the atomic orbital compositions calculated for the highest-occupied (HOMO) and lowest-unoccupied molecular orbital (LUMO) of the studied complexes. As the topology of the orbitals does not significantly differ along the series, only the molecular orbitals of the complexes with N^N = 6,6'-Cl$_2$bpy are displayed. As previously reported for this type of complexes,[10,58] the HOMO appears mainly centred over the metal and the phosphorus atoms, with small contributions from the phenyl rings, and the LUMO is exclusively located on the bpy ligand. As the HOMO is centred on a region of the complex that is structurally unaltered along the series containing the POP and xantphos P^P ligands, its energy only features small variations. All the HOMOs of the bpy-substituted complexes have energies in a range of 0.1 eV and are slightly more stable than those of the corresponding reference complexes, in good agreement with the experimental trends observed for the oxidation potentials (Table 2).

The evolution of the LUMOs is more complex (Fig. 3). As expected,[59,60] the attachment of the electron-withdrawing halogen substituents to the bpy ligand where the LUMO is located induces the stabilization of this orbital. The addition of a single Br atom stabilizes the LUMO by 0.15 and 0.09 eV (for POP and xantphos containing complexes, respectively), whereas the introduction of two Cl or Br atoms in the 6,6'-positions approximately doubles this stabilization, the effect being more pronounced for the [Cu(POP)(6,6'-Br$_2$bpy)]$^+$ complex.

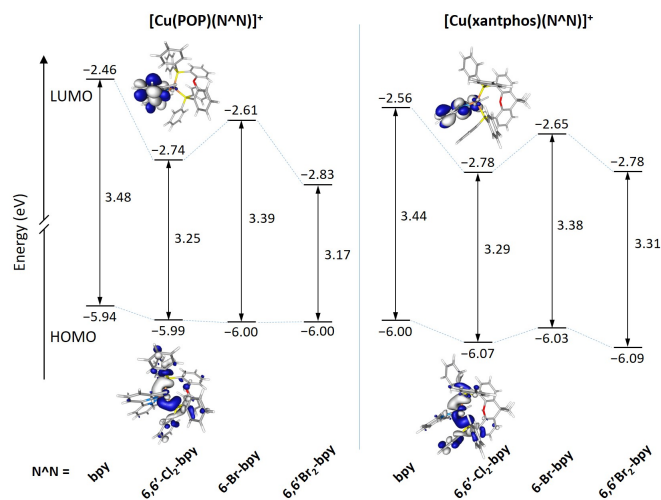**Fig. 3** Energy diagram displaying the energies calculated for the HOMO and LUMO of [Cu(POP)(N^N)]$^+$ and [Cu(xantphos)(N^N)]$^+$ complexes. The HOMO–LUMO energy gaps are also quoted. Isovalue contour plots (±0.03 e bohr^{-3}) are shown for the HOMO and LUMO of complexes with N^N = 6,6'-Cl$_2$-bpy.

The HOMO−LUMO gap of all the substituted complexes is narrower than that of the reference complexes, and decreases in passing from mono- to bis-halo-substituted complexes (Fig. 3). This HOMO−LUMO gap is usually employed as a first approach to predict the relative energy of the lowest-energy singlet (S_1) and triplet (T_1) excited states, which are generally described as originating from the HOMO → LUMO excitation in this type of complexes. Based on this assumption, it is to be expected that all the substituted complexes feature S_1 and T_1 at lower energies than the reference complexes, and thus exhibit absorption/emission wavelengths further towards the red. Among them, 6,6'-disubstituted complexes are expected to present a larger red shift than their monosubstiuted analogues. However, as discussed below, these predictions are useful to explain the absorption processes taking place at the ground state minimum-energy geometry (Frank-Condon region), but when studying emission processes, the geometry relaxation of the excited states, will affect in a great extent the order of the emission energies.

Photophysical properties and excited states

The solution absorption spectra of the complexes in CH$_2$Cl$_2$ are displayed in Fig. 4. In addition to high energy bands assigned to ligand-based transitions, the complexes show broad metal-to-ligand charge transfer (MLCT) bands in the range 350 to 470 nm, which are typical of [Cu(P^P)(bpy)][PF$_6$] complexes.[10,16] Values of λ_{max} for the MLCT bands depend on the bpy ligand but show no dependence on the P^P ligand (see Fig. S5†). The MLCT bands for the complexes with 6-Brbpy are the most blue-shifted, in good agreement with the larger HOMO−LUMO gaps predicted for these complexes (Fig. 3). A change from 6,6'-Br$_2$bpy to 6,6'-Cl$_2$bpy has little effect on λ_{max} of the MLCT bands.
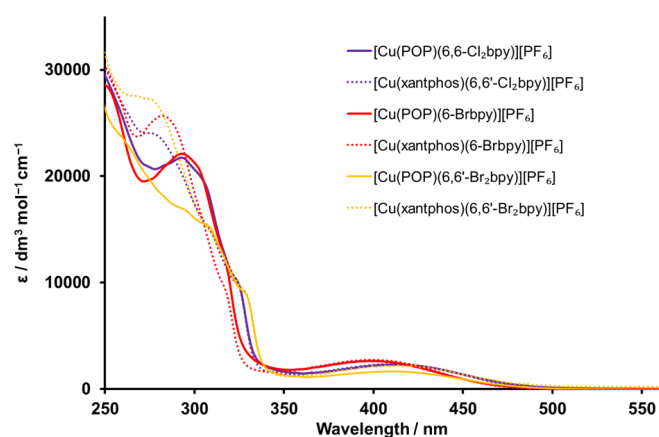
Fig. 4 Solution absorption spectra of the [Cu(P^P)(bpy)][PF$_6$] complexes (CH$_2$Cl$_2$, 2.5 × 10^{-5} mol dm^{-3}).

Table 3 Vertical excitation energies (E) calculated at the TD-DFT B3LYP/(6-31G*+LANL2DZ) level for the lowest singlet (S$_1$) and triplet (T$_1$) excited states of the [Cu(P^P)(N^N)]$^+$ complexes in CH$_2$Cl$_2$ solution. S$_0$→S$_1$ oscillator strengths (f) are given within parentheses. The energy of the T$_1$ state at its fully optimized TD-DFT geometry is given in the last column.

Complex cation	S$_1$	T$_1$	T$_1$ (relaxed)
	E (eV/nm) (f)	E (eV)	E (eV)
[Cu(POP)(bpy)]$^+$	3.089 / 401 (0.08)	2.906	1.582
[Cu(xantphos)(bpy)]$^+$	3.085 / 402 (0.09)	2.893	1.577
[Cu(POP)(6,6'-Cl$_2$bpy)]$^+$	2.833 / 438 (0.05)	2.704	1.718
[Cu(xantphos)(6,6'-Cl$_2$bpy)]$^+$	2.819 / 440 (0.06)	2.670	1.774
[Cu(POP)(6-Brbpy)]$^+$	2.949 / 420 (0.06)	2.773	1.662
[Cu(xantphos)(6-Brbpy)]$^+$	2.942 / 421 (0.08)	2.758	1.723
[Cu(POP)(6,6'-Br$_2$bpy)]$^+$	2.791 / 444 (0.04)	2.658	1.709
[Cu(xantphos)(6,6'-Br$_2$bpy)]$^+$	2.827 / 439 (0.06)	2.685	1.802

To further investigate the nature of the electronic states giving rise to the absorption spectra, the lowest-lying singlet and triplet excited states were calculated for all the complexes using the time-dependent DFT (TD-DFT) method. The vertical B3LYP/(6-31G**+LANL2DZ) excitation energies computed for S$_1$ and T$_1$ at the optimized geometry of S$_0$ are collected in Table 3. B3LYP/(def2svp+def2tzvp) calculations lead to identical trends, but underestimate the excitation energies (Table S3†). The main contribution (>95%) to S$_1$ and T$_1$ is in all cases the HOMO → LUMO monoexcitation, which implies an electron transfer from the Cu(P^P) environment to the bpy ligand (Fig. 3), thus supporting the MLCT character of these states. Since no other singlet state with significant oscillator strength (f > 0.01) appears above 350 nm, S$_1$ is responsible for the low-energy absorption band observed in the 350–450 nm region (Fig. 4). The energies predicted for the S$_0$→S$_1$ transition are in good accord with the experimental values of the low-energy absorption band and fully support the relative positions recorded for this band. The attachment of the halogen substituents shifts the absorption to the red compared to the unsubstituted reference complexes, the redshift being more pronounced for the 6,6'-substituted complexes with very little effect in changing from from 6,6'-Br$_2$bpy to 6,6'-Cl$_2$bpy (Table 3). The following transition with f > 0.01 mainly results from the HOMO→LUMO+1 monoexcitation (>95%) and also has an MLCT character. This transition is calculated around 330 nm and accounts for the shoulder observed on the low-energy side of the high-intensity band around 300 nm (Fig. 4). The bands below 300 nm mainly correspond to π→π* transitions involving the ligands. The theoretical spectra simulated for complexes with 6,6'-Cl$_2$bpy (Fig. S6†) perfectly reproduce the shape of the experimental spectra.

Fig. 5 Normalized solution emission spectra of [Cu(P^P)(bpy)][PF$_6$] complexes (CH$_2$Cl$_2$, 2.5 × 10^{-5} mol dm^{-3}). For λ_{exc} see Table 4.

The emission spectra of the complexes in solution (CH$_2$Cl$_2$, 2.5 × 10^{-5} mol dm^{-3}) are shown in Fig. 5 and the photophysical properties are summarized in Table 4. The complexes are emissive in the orange to red region with λ_{em}^{max} between 600 and 650 nm and the bands are structured with two emission maxima. As observed for the MLCT bands in the absorption spectra, the exchange of the P^P chelating ligand has little effect on the emission wavelength in solution. A small hypsochromic shift of the emission is observed for the halo-substituted complexes with respect to those with unsubstituted bpy (Table 4). Within the series of complexes, a bathochromic shift is observed for the emission maxima of the complexes containing 6-Brbpy with respect to those with 6,6'-Br$_2$bpy and 6,6'-Cl$_2$bpy (Fig. 5).

The relative ordering of the emission energies recorded for the [Cu(P^P)(bpy)][PF$_6$] complexes correlates neither with the order observed for the low-energy MLCT bands in the absorption spectra, nor with the order expected on the basis of

TD-DFT calculations or HOMO−LUMO gaps. The T_1 state for all the halo-substituted complexes is indeed calculated to be lower in energy than for the unsubstituted complexes (Table 3), and the former present a smaller HOMO−LUMO gap (Fig. 3). Therefore, as observed for the absorption, a bathochromic shift of the emission had to be expected upon halo-substitution, but the opposite is found experimentally (Table 4). To explain this behaviour, it should be remembered that absorption takes place at the optimal equilibrium geometry of S_0, at which HOMO−LUMO gaps and TD-DFT vertical excitation energies are calculated, whereas emission occurs at the T_1 relaxed geometry. As discussed above, Cu(I) complexes undergo a very important geometrical relaxation in the T_1 state because of the relative planarization of the tetrahedral structure. As a result, the T_1 state is largely stabilized and the emission energy of the $[Cu(P^{\wedge}P)(bpy)][PF_6]$ complexes (600–650 nm) is significantly lower than the absorption energy (400–450 nm).

Therefore, the emission energy is determined to a large extent by the geometry relaxation that the complex experiences in the T_1 state. The unsubstituted $[Cu(POP)(bpy)]^+$ and $[Cu(xantphos)(bpy)]^+$ complexes show the largest geometrical changes and present the lowest emission energies due to the greatest stabilization of the emitting state T_1 (Table 4). In contrast, relaxation of the tetrahedral geometry in 6,6'-halo-substituted complexes is impeded by the presence of the substituents and these complexes exhibit higher emission energies despite the decrease of the HOMO−LUMO gap. Complexes $[Cu(POP)(6\text{-Brbpy})]^+$ and $[Cu(xantphos)(6\text{-Brbpy})]^+$ with only one halogen atom exhibit intermediate emission energies (Table 4). This picture is fully confirmed when we compare the vertical TD-DFT energy calculated for T_1 at the S_0 optimal geometry, which should be related to absorption energies, with the energy calculated after full TD-DFT relaxation of the T_1 geometry (Table 3), which has to be related to emission energies. The T_1 state of the unsubstituted reference complexes undergoes a lessening of 1.32 eV upon relaxation, and these complexes present the lowest T_1 energy. For the 6,6'-halo-substituted complexes, the energy of T_1 decreases in a lower degree (0.9–1.0 eV) due to the restricted geometry relaxation, and these complexes have the highest T_1 energy. Intermediate values are obtained for the mono-substituted complexes $[Cu(POP)(6\text{-Brbpy})]^+$ and $[Cu(xantphos)(6\text{-Brbpy})]^+$ (Table 3). Therefore, the energy order predicted for the relaxed T_1 state perfectly matches the experimental emission energies in solution (Table 4).

The presence of two emission maxima in the bands of the solution spectra (Fig. 5) has also been reported for related $[Cu(P^{\wedge}P)(bpy)][PF_6]$ complexes.[9,10,16] A possible explanation for the double structure of the band is the coexistence of phosphorescence and TADF processes. Phosphorescence from T_1 would give rise to the redder component of the emission and TADF from S_1 would account for the component at higher energies. The energy difference between the fully-relaxed S_1 and T_1 states has been estimated via TD-DFT optimizations and ranges from 0.15 eV for complex $[Cu(POP)(6,6'\text{-Cl}_2bpy)]^+$ to 0.19 eV for $[Cu(xantphos)(6\text{-Brbpy})]^+$. As has been previously reported for similar Cu(I) complexes,[61,62] these energy differences are indeed small enough to allow TADF at room temperature.[17] Within each series, the energy difference between S_1 and T_1 is slightly higher for complexes with N^N = 6-Brbpy, making TADF less favourable for them, which could explain the smaller experimental intensities of the more hypsochromic maxima featured by these complexes (Fig. 5).

The complexes are weak emitters in solution, with the highest PLQY of 1.7% for a deaerated solution of $[Cu(POP)(6,6'\text{-Cl}_2bpy)][PF_6]$ (reduction of the amount of dissolved O_2 by a 20 min gas flow of argon through the solution). Comparison with the respective PLQY of $[Cu(xantphos)(6,6'\text{-Me}_2bpy)][PF_6]$ (10% upon deaeration)[58] indicates that chloro (and even less bromo) substituents in the 6,6'-positions of the bpy ligand are not as efficient at enhancing the emissive properties of $[Cu(P^{\wedge}P)(bpy)][PF_6]$ complexes as methyl groups. It is, however, unclear if this is due to additional or enhanced non-radiative pathways caused by the halo-substitution. The lifetime (τ) values measured in solution are of the order of hundreds of ns and are compatible with the coexistence of phosphorescent and TADF emission.

Table 4 Emission maxima, photoluminescence quantum yields (PLQY) and lifetimes (τ) for $[Cu(P^{\wedge}P)(N^{\wedge}N)][PF_6]$ complexes

Complex cation	CH$_2$Cl$_2$ solution[a]				Powder[b]			Frozen glass (Me-THF, 77K)		
	λ_{exc} [nm]	λ_{em}^{max} [nm]	PLQY (non-deaerated / deaerated) [%]	τ (non-deaerated / deaerated) [ns]	λ_{em}^{max} [nm]	PLQY [%]	τ [µs]	$\lambda_{em}^{max\ d}$ [nm]	PLQY^e [%]^e	τ^d [µs]
$[Cu(POP)(bpy)]^{+f}$	390	618, 649	0.4/0.5	43/46[b]	580	3.0	1.5	610	6.0	16
$[Cu(xantphos)(bpy)]^{+f}$	390	620, 650	0.5/0.5[b]	75/104[b]	587	1.7	1.3	613	3.0	11
$[Cu(POP)(6,6'\text{-Cl}_2bpy)]^+$	400	611, 636	0.9/1.7[c]	218/372[c]	584	14.8	2.7	573	25.7	82
$[Cu(xantphos)(6,6'\text{-Cl}_2bpy)]^+$	400	605, 629	0.7/0.9[c]	115/138[c]	587	17.1	3.3	560	30.6	119
$[Cu(POP)(6\text{-Brbpy})]^+$	400	618, 641	0.6/0.8[c]	159/239[c]	582	3.9	2.5	613	3.8	12
$[Cu(xantphos)(6\text{-Brbpy})]^+$	400	617, 640	0.5/0.6[c]	155/217[c]	569	16.3	4.8	593	18.0	25
$[Cu(POP)(6,6'\text{-Br}_2bpy)]^+$	400	608, 636	0.6/0.8	90/107	596	6.3	2.6	568	27.5	55
$[Cu(xantphos)(6,6'\text{-Br}_2bpy)]^+$	400	601, 632	0.5/0.6[c]	38/38[c]	544	10.9	2.3	569	40.0	107

[a] Solution concentration = 2.5×10^{-5} mol dm^{-3}. [b] λ_{exc} = 365 nm. [c] λ_{exc} = 405 nm. [d] λ_{exc} = 410 nm. [e] λ_{exc} = 320 nm. [f] Complexes published.[58]

In the solid state, [Cu(POP)(6,6'-Cl$_2$bpy)][PF$_6$], [Cu(xantphos)(6,6'-Cl$_2$bpy)][PF$_6$], [Cu(xantphos)(6-Brbpy)][PF$_6$] and [Cu(xantphos)(6,6'-Br$_2$bpy)][PF$_6$] show the highest PLQYs. However, with 11 to 17%, the values are moderate in comparison with complexes that have methyl groups in the 6,6'-positions at the bpy ligand (e.g. 37% for [Cu(xantphos)(6,6'-Me$_2$bpy)][PF$_6$]).[58] The complexes are yellow to orange emitters in the solid state (Fig. 6). The blue-shift on going from solution to powder (Table 4) is typically observed for these [Cu(P^P)(N^N)]$^+$ cations and can be explained in terms of the rigidity of the environment in the solid state, which severely restricts the geometrical relaxation discussed above for the emitting T$_1$ state. The influence of the bisphosphane ligand on the photophysical properties in the solid state strongly depends on the bpy ligand. For the complexes with 6,6'-Cl$_2$bpy, the emission maxima are similar for both the POP and xantphos complexes, and the PLQY values are of the same order of magnitude. In the complexes with 6-Brbpy, the effects of the phosphane ligands differ strongly; [Cu(xantphos)(6-Brbpy)][PF$_6$] emits at higher energy and also has a much higher PLQY (16.3%) than the respective complex with POP (3.9%). For the compounds with 6,6'-Br$_2$bpy, the PLQY values are of the same order of magnitude for both complexes, although the emission maximum is strongly blue-shifted for the xantphos complex (544 nm vs. 596 nm for [Cu(POP)(6,6'-Br$_2$bpy)][PF$_6$]). In the solid-state emission spectra, only [Cu(xantphos)(6-Brbpy)][PF$_6$] and [Cu(xantphos)(6,6'-Br$_2$bpy)][PF$_6$] show a noteworthy blue-shift compared to the complexes with unsubstituted bpy. However, we note that packing interactions have a strong influence on the geometry relaxation of the emitting state and, therefore, on the solid state emission maxima, and that the observed effects are most probably due to geometrical effects.
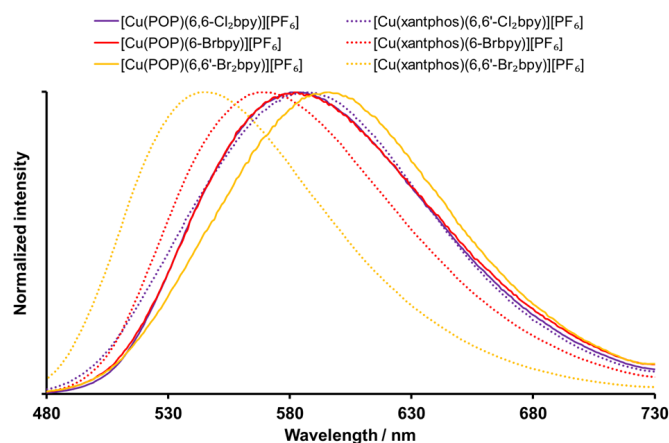

Fig. 6. Normalized emission spectra of solid [Cu(P^P)(N^N)][PF$_6$] complexes. For λ_{exc} see Table 4.

To further investigate the emission processes, the low-temperature emission spectra of the complexes were recorded in frozen solutions of Me-THF at 77 K (Fig. S7†). The PLQYs of the complexes are significantly enhanced compared to those in powder at room temperature, but for complexes with 6-Brbpy and 6,6'-Br$_2$bpy, the values remain mainly unaltered. The maximum PLQY of 40.0% was achieved for [Cu(xantphos)(6,6'-Br$_2$bpy)][PF$_6$] (Table 4). At the same time, the lifetimes of all the complexes are significantly extended with respect to the values in powder, with the longest lifetimes of 119 μs for [Cu(xantphos)(6,6'-Cl$_2$bpy)][PF$_6$] and 107 μs for [Cu(xantphos)(6,6'-Br$_2$bpy)][PF$_6$]. At 77 K, the thermal population of S$_1$ from T$_1$ is more difficult and TADF would be reduced or even completely impeded, pointing to the slower phosphorescence as the main contributor to the emission in agreement with the higher τ values. The emission maxima are red-shifted with respect to powder only for the complexes with unsubstituted bpy and 6-Brbpy and for [Cu(xantphos)(6,6'-Br$_2$bpy)][PF$_6$], but not for the complexes with 6,6'-Cl$_2$bpy and for [Cu(POP)(6,6'-Br$_2$bpy)][PF$_6$]. This might be due to the degree of geometry relaxation achieved by the emitting T$_1$ state in frozen Me-THF and in powder.

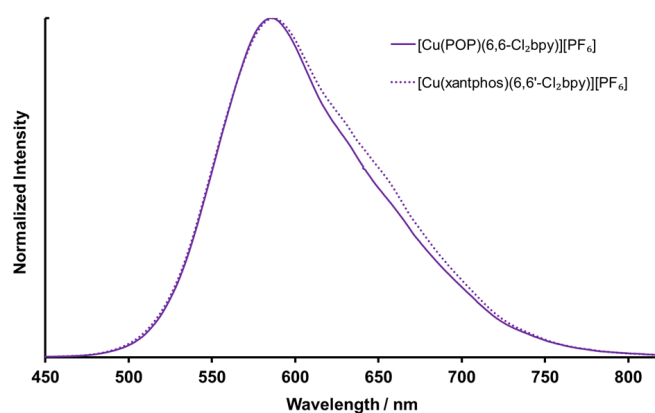**Fig. 7** Electroluminescence (EL) spectra for ITO/PEDOT:PSS/[Cu(P^P)(6,6'-Cl$_2$bpy)][PF$_6$]:[Emim][PF$_6$] 4:1/Al LECs operated at pulsed current (average density current 100 A m^{-2}, 1 kHz, 50% duty cycle, block wave).

Device properties

The series of compounds were tested in LECs in a double layer architecture, using PEDOT:PSS and the emissive layer sandwiched between ITO and aluminium electrodes. The active layer contained the respective copper(I) complex mixed with the ionic liquid [Emim][PF$_6$] with a molar ratio of 4:1 (Cu complex:IL). LECs were operated using a block-wave pulsed current of either 50 or 100 A m^{-2} (1 kHz and 50% duty cycle). Despite their promising photoluminescence properties, the bromo-substituted complexes did not show any electroluminescence. This phenomenon is still not well understood, but it is in line with previous reports on similar Cu(I)[16] and even Ir(III)[63] complexes. Considering the high PLQY and the absence of electroluminescence, the incorporation of heavier halo-substituents probably has a detrimental effect on charge transport. On the other hand, both [Cu(POP)(6,6'-Cl$_2$bpy)][PF$_6$] and [Cu(xantphos)(6,6'-Cl$_2$bpy)][PF$_6$] show very similar yellow electroluminescence with maxima at 586 and 587 nm, respectively (Fig. 7). The electroluminescence is similar to the photoluminescence of thin

Table 5 Performance of ITO/PEDOT:PSS/[Cu(P^P)^N^N)][PF$_6$]:[Emim][PF$_6$] 4:1 molar ratio/Al LECs measured using a pulsed current driving (average current density 50 and 100 A m^{-2}, 1 kHz, 50% duty cycle, block wave).

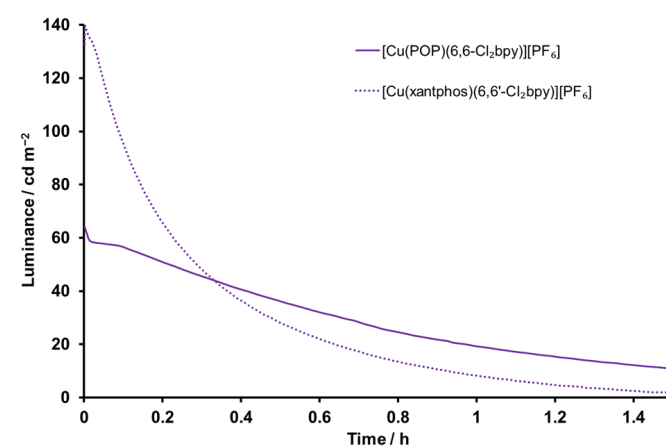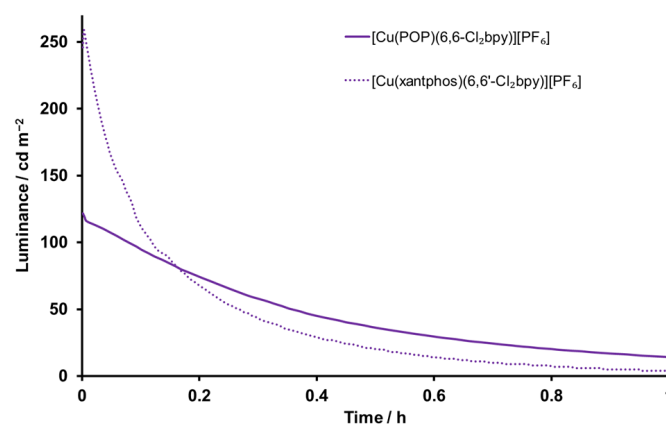| Complex	Avg. current density [A m^{-2}]	t_{on}[a] [s]	Lum$_0$[b] [cd m^{-2}]	Lum$_{max}$[c] [cd m^{-2}]	$t_{1/2}$[d] [min]	EQE$_{max}$[e] [%]	PCE$_{max}$[f] [lm W^{-1}]	Efficacy$_{max}$ [cd A^{-1}]	λ_{EL}^{max} [nm]
[Cu(POP)(6,6'-Cl$_2$bpy)][PF$_6$]	50	<5	64	64	35	0.6	0.3	1.3	586
[Cu(POP)(6,6'-Cl$_2$bpy)][PF$_6$]	100	<5	121	121	17	0.5	0.3	1.2	586
[Cu(xantphos)(6,6'-Cl$_2$bpy)][PF$_6$]	50	12	133	140	11	1.2	0.7	2.8	587
[Cu(xantphos)(6,6'-Cl$_2$bpy)][PF$_6$]	100	12	246	259	5	1.2	0.6	2.7	587

[a] Time to reach the maximum luminance. [b] Initial luminance. [c] Maximum luminance reached. [d] Time to reach one-half of the maximum luminance. [e] Maximum external quantum efficiency reached. [f] Maximum power conversion efficiency reached.

films of the same composition as the active layer of the LEC (Fig. S8†), with λ_{em}^{max}= 581 nm for [Cu(POP)(6,6'-Cl$_2$bpy)][PF$_6$] and 589 nm for [Cu(xantphos)(6,6'-Cl$_2$bpy)][PF$_6$]. The corresponding PLQYs, 7.5% for the POP and 10.5% for the xantphos containing complex, are lower than in the powders, which is attributed to the higher flexibility of the complexes in the presence of the ionic liquid.

The devices show very fast turn-on times (t_{on}), acceptable luminance but relatively poor stability (Fig. 8, 9, S9†, S10† and Table 5). The extremely short turn on times are especially noteworthy, with only 12 s or less needed to reach the maximum luminance. For the device employing [Cu(xantphos)(6,6'-Cl$_2$bpy)][PF$_6$], the maximum luminance (Lum$_{max}$) values are higher (140 and 259 cd m^{-2} measured at 50 and 100 A m^{-2}, respectively) than for the respective complex with POP (64 and 121 cd m^{-2}), which is consistent with the higher PLQY values of the former. In comparison, the device with [Cu(xantphos)(6,6'-Me$_2$bpy)][PF$_6$] has a slightly higher Lum$_{max}$ value and better efficiency (145 cd m^{-2} and 3.0 cd A^{-1}, respectively).[10] However, this complex has a significantly higher PLQY in a thin film (21.8%) as compared to the chloro-complexes (7.5 and 10.5%). Considering these thin film PLQY values together with an outcoupling efficiency of 20%, [Cu(POP)(6,6'-Cl$_2$bpy)][PF$_6$] and [Cu(xantphos)(6,6'-Cl$_2$bpy)][PF$_6$] have a theoretical maximum EQE of 1.5% and 2.0 %. The observed EQE values for the devices operated at 100 A m^{-2} are 1.2% for both complexes, which is equivalent to 80 and 60% of the respective theoretical maximum. Hence, considering the thin film PLQYs, the devices employing the complexes with 6,6'-Cl$_2$bpy perform significantly better than with [Cu(xantphos)(6,6'-Me$_2$bpy)][PF$_6$]. In the complexes with 6,6'-Cl$_2$bpy, the lifetimes $t_{1/2}$ are longer for the POP analogue (35 and 17 minutes *vs*. 11 and 5 minutes). A similar trend, but with much better performance, has been observed for complexes with 6-Etbpy where the device with [Cu(xantphos)(6-Etbpy)][PF$_6$] gave the higher luminance, but shorter lifetime (77 cd m^{-2} and 51 hours) in comparison to [Cu(POP)(6-Etbpy)][PF$_6$] (53 cd m^{-2} and 82 hours).[10] For the device with [Cu(xantphos)(6,6'-Cl$_2$bpy)][PF$_6$], although the maximum luminance is comparable to that of [Cu(xantphos)(6,6'-Me$_2$bpy)][PF$_6$], the device lifetime is even shorter (11 min vs. 48 min, both at 50 A m^{-2}). These results illustrate again the previously observed trade-off between either

a brightly shining or long-living device.[10] Although substitution of the bpy ligand with chloro-substituents in the 6,6'-positions is detrimental to the device lifetime, we have shown the positive effects on the turn-on time and efficiency of the devices.

Fig. 8 Luminance versus time characteristics for ITO/PEDOT:PSS/[Cu(P^P)(6,6'-Cl$_2$bpy)][PF$_6$]:[Emim][PF$_6$] 4:1/Al LECs operated at pulsed current (average current density 50 A m^{-2}, 1 kHz, 50% duty cycle, block wave).

Fig. 9 Luminance versus time characteristics for ITO/PEDOT:PSS/[Cu(P^P)(6,6'-Cl$_2$bpy)][PF$_6$]:[Emim][PF$_6$] 4:1/Al LECs operated at pulsed current (average current density 100 A m^{-2}, 1 kHz, 50% duty cycle, block wave).

Conclusions

We have reported six [Cu(P^P)(bpy)][PF$_6$] complexes containing chloro- and bromo-substituted bpy ligands. The single crystal structures of [Cu(POP)(6,6'-Cl$_2$bpy)][PF$_6$], [Cu(xantphos)(6,6'-Cl$_2$bpy)][PF$_6$]·CH$_2$Cl$_2$, [Cu(POP)(6-Brbpy)][PF$_6$] and [Cu(xantphos)(6-Brbpy)][PF$_6$]·0.7Et$_2$O confirm that all the complexes are coordinated in a distorted tetrahedral geometry. High-pressure single crystal X-ray experiments for [Cu(POP)(6-Brbpy)][PF$_6$] reveal the robustness of the complex geometry under pressures up to 4.5 GPa.

The electron-withdrawing halo-substituents shift the Cu$^+$/Cu^{2+} oxidation potentials to higher potentials (+0.90 to +0.98 V) compared to complexes with unmodified bpy (+0.72 or 0.76 V). Comparison of the solution PLQYs (1.7% and lower) with that of [Cu(xantphos)(6,6'-Me$_2$bpy)][PF$_6$] (10%)[10] shows that halogen atoms in the 6,6'-positions of the bpy ligand are not as efficient at enhancing the emissive properties of [Cu(P^P)(bpy)][PF$_6$] complexes as methyl groups. This might be due to additional radiative pathways offered by the halogens.

The LECs employing the [Cu(POP)(6,6'-Cl$_2$bpy)][PF$_6$] and [Cu(xantphos)(6,6'-Cl$_2$bpy)][PF$_6$] complexes have fast turn on times (<12 s), in particular when compared to the reference LECs with [Cu(POP)(6,6'-Me$_2$bpy)][PF$_6$] (23 min)[9] and [Cu(xantphos)(6,6'-Me$_2$bpy)][PF$_6$] (10 min).[10] The maximum luminance values are similar, with 140 cd m^{-2} for [Cu(xantphos)(6,6'-Cl$_2$bpy)][PF$_6$] vs. 145 cd m^{-2} for [Cu(xantphos)(6,6'-Me$_2$bpy)][PF$_6$]. This is especially noteworthy taking into account the corresponding PLQY values in thin films, which are significantly higher for [Cu(xantphos)(6,6'-Me$_2$bpy)][PF$_6$] (21.8%) as compared to the complexes with 6,6'-Cl$_2$bpy (7.5 and 10.5%, respectively). As a result, the devices using copper(I) complexes with 6,6'-Cl$_2$bpy perform at about 60 and 80% of their theoretical EQE, respectively, which is remarkable for simple single-layer electroluminescent devices. We observed a detrimental effect of the bromo-substitution, hindering the charge transport within the active layer and resulting in the absence of electroluminescence. Substitution with the chlorine atoms undermines the device stability, but further studies are needed to rationalize the cause of this behavior, which might originate from the oxidation of the complex, dissociation of the ligand or other electrochemical processes in the cell.

In future studies, we will explore bpy ligands that combine alkyl and halo-substituents, and will also investigate the effects of introducing halogen atoms in different substituent positions.

Acknowledgements

Notes and references

^{a}Department of Chemistry, University of Basel, BPR 1096, Mattenstrasse 24a, CH-4058 Basel, Switzerland. E-mail: catherine.housecroft@unibas.ch
^{b}Instituto de Ciencia Molecula, Universidad de Valencia, 46980 Paterna (Valencia), Spain. E-mail: enrique.orti@uv.es

1 H. Rudmann, S. Shimada and M. F. Rubner, *J. Am. Chem. Soc.*, 2002, **124**, 4918.

2 C. M. Elliott, F. Pichot, C. J. Bloom and L. S. Rider, *J. Am. Chem. Soc.*, 1998, **120**, 6781.

3 R. D. Costa, E. Ortí, H. J. Bolink, F. Monti, G. Accorsi and N. Armaroli, *Angew. Chem. Int. Ed.*, 2012, **51**, 8178.

4 F. Dumur, *Org. Electronics*, 2015, **21**, 27.

5 M. Magni, P. Biagini, A. Colombo, C. Dragonetti, D. Roberto and A. Valore, *Coord. Chem. Rev.*, 2016, **322**, 69.

6 D. G. Cuttell, S.-M. Kuang, P. E. Fanwick, D. R. McMillin and R. A. Walton, *J. Am. Chem. Soc.*, 2002, **124**, 6.

7 S.-M. Kuang, D. G. Cuttell, D. R. McMillin, P. E. Fanwick and R. A. Walton, *Inorg. Chem.*, 2002, **41**, 3313.

8 R. D. Costa, D. Tordera, E. Ortí, H. J. Bolink, J. Schönle, S. Graber, C. E. Housecroft, E. C. Constable and J. A. Zampese, *J. Mater. Chem.* 2011, **21**, 16108.

9 S. Keller, E. C. Constable, C. E. Housecroft, M. Neuburger, A. Prescimone, G. Longo, A. Pertegás, M. Sessolo and H. J. Bolink, *Dalton Trans.*, 2014, **43**, 16593.

10 S. Keller, A. Pertegás, G. Longo, L. Martinez, J. Cerdá, J. M. Junquera-Hernández, A. Prescimone, E. C. Constable, C. E. Housecroft, E. Ortí and H. J. Bolink, *J. Mater. Chem. C*, 2016, **4**, 3857.

11 R. Czerwieniec and H. Yersin, *Inorg. Chem.*, 2015, **54**, 4322.

12 D. Asil, J. A. Foster, A. Patra, X. de Hatten, J. del Barrio, O. A. Scherman, J. R. Nitschke and R. H. Friend, *Angew. Chem. Int. Ed.*, 2014, **53**, 8388.

13 N. Armaroli, G. Accorsi, M. Holler, O. Moudam, J.-F. Nierengarten, Z. Zhou, R. T. Wegh and R. Welter, *Adv. Mater.*, 2006, **18**, 1313.

14 C. Bizzarri, C. Strabler, J. Prock, B. Trettenbrein, M. Ruggenthaler, C.-H. Yang, F. Polo, A. Iordache, P. Brüggeller and L. De Cola, *Inorg. Chem.*, 2014, **53**, 10944.

15 M. D. Weber, C. Garino, G. Volpi, E. Casamassa, M. Milanesio, C. Barolo and R. D. Costa, *Dalton Trans.*, 2016, **45**, 8984.

16 F. Brunner, L. Martínez-Sarti, S. Keller, A. Pertegás, A. Prescimone, E. C. Constable, H. J. Bolink and C. E. Housecroft, *Dalton Trans.*, 2016, **45**, 15180.

17 R. Czerwieniec, M. J. Leitl, H. H. H. Homeier and H. Yersin, *Coord. Chem. Rev.*, 2016, **325**, 2.

18 D. Volz, D. M. Zink, T. Bocksrocker, J. Friedrichs, M. Nieger, T. Baumann, U. Lemmer and S. Bräse, *Chem. Mater.*, 2013, **25**, 3414.

19 D. Volz, Y. Chen, M. Wallesch, R. Liu, C. Fléchon, D. M. Zink, J. Friedrichs, H. Flügge, R. Steininger, J. Göttlicher, C. Heske, L. Weinhardt, S. Bräse, F. So and T. Baumann, *Adv. Mater.*, 2015, **27**, 2538.

20 M. J. Leitl, F.-R. Küchle, H. A. Mayer, L. Wesemann and H. Yersin, *J. Phys. Chem. A*, 2013, **117**, 11823.

21 H. Ohara, A. Kobayashia and M. Kato, *Dalton Trans.*, 2014, **43**, 17317.

22 A. Tsuboyama, K. Kuge, M. Furugori, S. Okada, M. Hoshino and K. Ueno, *Inorg. Chem.*, 2007, **46**, 1992.

23 M. D. Ward, S. M. Couchman and J. C. Jeffery, *Acta Cryst.*, 1998, **54**, 1820.

24 M. G. Fraser, H. van der Salm, S. A. Cameron, A. G. Blackman and K. C. Gordon, *Inorg. Chem.*, 2013, **52**, 2980.

25 M. Schmittel, C. Michel, S.-X. Liu, D. Schildbach and D. Fenske, *Eur. J. Inorg. Chem.*, 2001, 1155.

26 C. C. L. McCrory, X. Ottenwaelder, T. D. P. Stack and C. E. D. Chidsey, *J. Phys. Chem. A*, 2007, **111**, 12641.

27 C. J. Hawkins and D. D. Perrin, *J. Chem Soc.*, 1963, 2996.

28 D. J. Casadonte and D. R. McMillin, *J. Am. Chem. Soc.*, 1987, **109**, 331.

29 D. T. Clark, J. N. Murrell and J. M. Tedder, *J. Chem. Soc.*, 1963, 1250.

30 E. C. Constable and K. R. Seddon, *Tetrahedron*, 1983, **39**, 291.

31 G. J. Kubas, *Inorg. Synth.*, 1979, **19**, 90.

32 Bruker Analytical X-ray Systems, Inc., 2006, APEX2, version 2 User Manual, M86-E01078, Madison, WI.

33 P. W. Betteridge, J. R. Carruthers, R. I. Cooper, K. Prout and D. J. Watkin, *J. Appl. Cryst.*, 2003, **36**, 1487.

34 A. L. Spek, *Acta Cryst. C*, 2015, **71**, 9.

35 I. J. Bruno, J. C. Cole, P. R. Edgington, M. K. Kessler, C. F. Macrae, P. McCabe, J. Pearson and R. Taylor, *Acta Crystallogr., Sect. B*, 2002, **58**, 389.

36 C. F. Macrae, I. J. Bruno, J. A. Chisholm, P. R. Edgington, P. McCabe, E. Pidcock, L. Rodriguez-Monge, R. Taylor, J. van de Streek and P. A. Wood, *J. Appl. Cryst.*, 2008, **41**, 466.

37 S. A. Moggach, D. R. Allan, S. Parsons and J. E. Warren, *J. Appl. Cryst.*, 2008, **41**, 249.

38 I. Kantor, V. Prakapenka, A. Kantor, P. Dera, A. Kurnosov, S. Sinogeikin, N. Dubrovinskaia and L. Dubrovinsky, *Rev. Sci. Instrum.*, 2012, **83**, 125102.

39 D. M. Adams, R. Appleby and S. K. Sharma, *J. Phys. E: Sci. Instrum.*, 1976, **9**, 1140.

40 CrysAlisPro 1.171.38.41k (Rigaku OD, 2015)

41 Gaussian 16, Revision A.03, M. J. Frisch, G. W. Trucks, H. B. Schlegel, G. E. Scuseria, M. A. Robb, J. R. Cheeseman, G. Scalmani, V. Barone, G. A. Petersson, H. Nakatsuji, X. Li, M. Caricato, A. V. Marenich, J. Bloino, B. G. Janesko, R. Gomperts, B. Mennucci, H. P. Hratchian, J. V. Ortiz, A. F. Izmaylov, J. L. Sonnenberg, D. Williams-Young, F. Ding, F. Lipparini, F. Egidi, J. Goings, B. Peng, A. Petrone, T. Henderson, D. Ranasinghe, V. G. Zakrzewski, J. Gao, N. Rega, G. Zheng, W. Liang, M. Hada, M. Ehara, K. Toyota, R. Fukuda, J. Hasegawa, M. Ishida, T. Nakajima, Y. Honda, O. Kitao, H. Nakai, T. Vreven, K. Throssell, J. A. Montgomery, Jr., J. E. Peralta, F. Ogliaro, M. J. Bearpark, J. J. Heyd, E. N. Brothers, K. N. Kudin, V. N. Staroverov, T. A. Keith, R. Kobayashi, J. Normand, K. Raghavachari, A. P. Rendell, J. C. Burant, S. S. Iyengar, J. Tomasi, M. Cossi, J. M. Millam, M. Klene, C. Adamo, R. Cammi, J. W. Ochterski, R. L. Martin, K. Morokuma, O. Farkas, J. B. Foresman and D. J. Fox, Gaussian, Inc., Wallingford CT, **2016**.

42 C. Lee, W. Yang and R.G. Parr, *Phys. Rev. B*, 1988, **37**, 785.

43 A. D. Becke, *J. Chem. Phys.*, 1993, **98**, 5648.

44 F. Weigend and R. Ahlrichs, *Phys. Chem. Chem. Phys.*, 2005, **7**, 3297.

45 F. Weigend, *Phys. Chem. Chem. Phys.*, 2006, 8, 1057.

46 S. Grimme, J. Antony, S. Ehrlich and H. Krieg, *J. Chem. Phys.*, 2010, **132**, 154104.

47 S. Grimme, S. Ehrlich and L. Goerigk, *J. Comput. Chem.*, 2011, **32**, 1456.

48 M. Petersilka, U. J. Gossmann and E. K. U. Gross, *Phys. Rev. Lett.*, 1996, **76**, 1212.

49 C. Jamorski, M. E. Casida and D. R. Salahub, *J. Chem. Phys.*, 1996, **104**, 5134.

50 M. E. Casida, C. Jamorski, K. C. Casida and D. R. Salahub, *J. Chem. Phys.*, 1998, **108**, 4439.

51 M. M. Francl, W. J. Pietro, W. J. Hehre, J. S. Binkley, M. S. Gordon, D. J. DeFrees and J. A. Pople, *J. Chem. Phys.*, 1982, **77**, 3654.

52 P. J. Hay and W. R. Wadt, *J. Chem. Phys.*, 1985, **82**, 299.

53 J. Tomasi and M. Persico, *Chem. Rev.*, 1994, **94**, 2027.

54 C. J. Cramer and D. G. Truhlar, in Solvent Effects and Chemical Reactivity. O. Tapia and J. Bertrán (Eds.), Kluwer, 1996, pp. 1–80.

55 J. Tomasi, B. Mennucci and R. Cammi, *Chem. Rev.*, 2005, **105**, 2999.

56 R. D. Costa, D. Tordera, E. Ortí, H. J. Bolink, J. Schönle, S. Graber, C. E. Housecroft, E. C. Constable and J. A. Zampese, *J. Mater. Chem.,* 2011, **21**, 16108.

57 C. Janiak, *J. Chem. Soc., Dalton Trans.*, 2000, 3885.

58 S. Keller, F. Brunner, J. M. Junquera, A. Pertegás, M.-G. La-Placa, A. Prescimone, E. C. Constable, H. J. Bolink, E. Ortí and C. E. Housecroft, *ChemPlusChem*, 2018, DOI: 10.1002/cplu.201700501.

59 A. F. Henwood and E. Zysman-Colman, *Top. Curr. Chem.* , 2016, **374**, 36.

60 S. B. Meier, W. Sarfert, J. M. Junquera-Hernández, M. Delgado, D. Tordera, E. Ortí, H. J. Bolink, F. Kessler, R. Scopelliti, M. Grätzel, M. K. Nazeeruddin and E. Baranoff, *J. Mater. Chem. C*, 2013, **1**, 58.

61 M. Y. Wong, E. Zysman-Colman in *Light-Emitting Electrochemical Cells*, ed. R. D. Costa, Springer International Publishing AG, Cham, Switzerland, 2017, pp. 237-266.

62 M. Elie, S. Gaillard, J.-L. Renaud, in *Light-Emitting Electrochemical Cells*, ed. R. D. Costa, Springer International Publishing AG, Cham, Switzerland, 2017, pp. 287-327.

63 A. M. Bünzli, H. J. Bolink, E. C. Constable, C. E. Housecroft, M. Neuburger, A. Pertegás and J. A. Zampese, *Eur. J. Inorg. Chem.,* 2012, 3780.

Luminescent Cu(I) complexes with bisphosphane and halogen-substituted 2,2'-bipyridine ligands

Sarah Keller,[a] Alessandro Prescimone,[a] Henk Bolink,[b] Michele Sessolo,[b] Giulia Longo,[b] Laura Martínez-Sarti,[b] José M. Junquera-Hernández,[b] Edwin C. Constable,[a] Enrique Ortí*[b] and Catherine E. Housecroft*[a]

[a]Department of Chemistry, University of Basel, BPR 1096, Mattenstrasse 24a, CH-4058 Basel, Switzerland; email: catherine.housecroft@unibas.ch
[b]Instituto de Ciencia Molecular, Universidad de Valencia, 46980 Paterna (Valencia), Spain; email: enrique.orti@uv.es
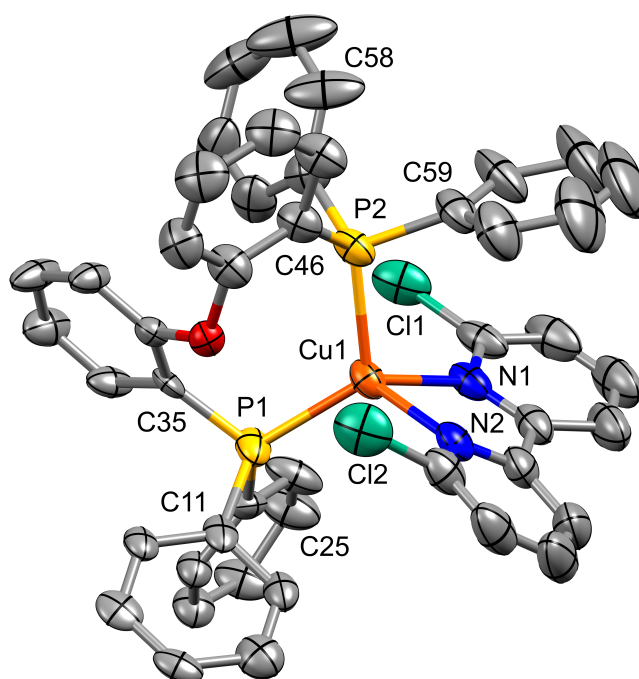
Fig. S1 Structure of the [Cu(POP)(6,6'-Cl$_2$bpy)]$^+$ cation in [Cu(POP)(6,6'-Cl$_2$bpy)][PF$_6$]. The POP ligand is disordered over two sites (50:50 occupancies) and only one site is shown; four disordered aromatic rings were refined as rigid bodies. Ellipsoids plotted at 50% probability level, H atoms omitted.
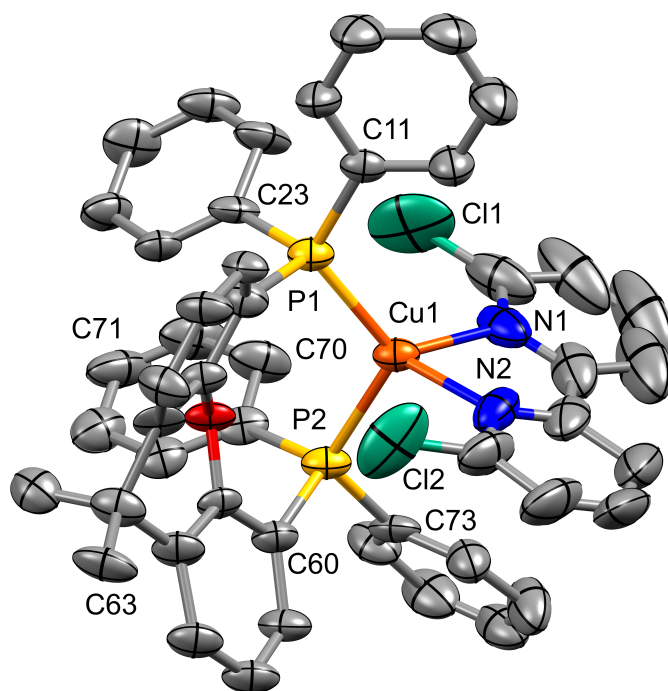
Fig. S2 Structure of the [Cu(xantphos)(6,6'-Cl$_2$bpy)]$^+$ cation in [Cu(xantphos)(6,6'-Cl$_2$bpy)][PF$_6$]·CH$_2$Cl$_2$. The xantphos ligand is disordered over two sites (50:50 occupancies). Ellipsoids plotted at 50% probability level, H atoms omitted.
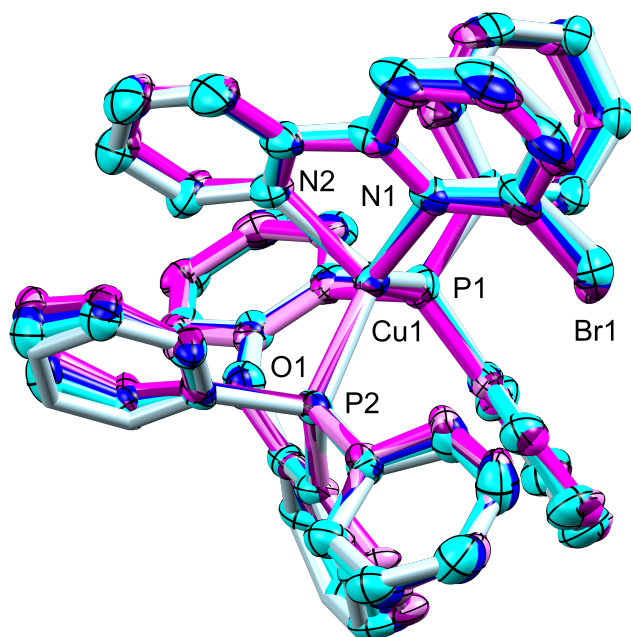

Fig. S3 Structure of the [Cu(POP)(6-Brbpy)]$^+$ cation in [Cu(POP)(6-Brbpy)][PF$_6$] under increasing pressure (0.16 to 4.5 GPa). Colour change from violet to light blue with increasing pressure. H atoms omitted, and ellipsoids are plotted at 50% probability level except for the highest pressure (4.5 GPa) structure which was refined anisotropically. The Cu–N and Cu–P bond distances decrease slightly as the pressure increases; e.g. Cu1–P1 changes from 2.250(6) Å at 0.16 GPa to 2.170(3) Å at 4.5 GPa, and Cu1–N2 from 2.110(14) to 2.017(4) Å, and the angle between the planes of the CuP$_2$ and CuN$_2$ units decreases from 83.63° to 86.09°.

Table S1 Experimental details for ambient and high pressure single crystal X-ray diffraction measurements performed on [Cu(POP)(6-Brbpy)][PF$_6$].

For all the structures: C$_{46}$H$_{35}$BrCuF$_6$N$_2$OP$_3$, M_r = 982.16, monoclinic, $P2_1/c$, Z = 4.

	P$_0$			
CCDC code	1535141	1584757	1584754	1584752
Crystal data				
Temperature (K)	123	293	293	293
Pressure (GPa)	ambient	0.16	1.30	1.80
a, b, c (Å)	15.3402 (6), 14.2344 (5), 19.2659 (7)	15.459 (10), 14.2430 (12), 19.413 (8)	15.123 (8), 13.6502 (10), 18.868 (7)	14.960 (8), 13.2757 (8), 18.724 (6)
β (°)	90.9159 (12)	90.03 (6)	91.32 (5)	92.23 (5)
V (Å^3)	4206.34 (15)	4274 (3)	3894 (2)	3716 (2)
D_x (Mg m^{-3})	1.551	1.526	1.675	1.755
Radiation type	Cu Ka	Synchrotron, l = 0.48590 Å	Synchrotron, l = 0.48590 Å	Synchrotron, l = 0.48590 Å
m (mm^{-1})	3.49	1.62	1.78	1.87
Crystal size (mm)	0.12 × 0.10 × 0.08	0.04 × 0.02 × 0.02	0.04 × 0.02 × 0.02	0.04 × 0.02 × 0.02
Data collection				
Diffractometer	Bruker Kappa Apex2	Pilatus 300K	Pilatus 300K	Pilatus 300K
Radiation source	Cu Ka	Diamond Light Source Beamline I19	Diamond Light Source Beamline I19	Diamond Light Source Beamline I19
Monochromator	Graphite	Double crystal Silicon 111	Double crystal Silicon 111	Double crystal Silicon 111
Absorption correction	Multi-scan *SADABS* (Siemens, 1996)	Multi-scan *CrysAlis PRO* 1.171.38.41 (Rigaku Oxford Diffraction, 2015) Empirical absorption correction using spherical harmonics, implemented in SCALE3 ABSPACK scaling algorithm.	Multi-scan *CrysAlis PRO* 1.171.38.41 (Rigaku Oxford Diffraction, 2015) Empirical absorption correction using spherical harmonics, implemented in SCALE3 ABSPACK scaling algorithm.	Multi-scan *CrysAlis PRO* 1.171.38.41 (Rigaku Oxford Diffraction, 2015) Empirical absorption correction using spherical harmonics, implemented in SCALE3 ABSPACK scaling algorithm.
T_{min}, T_{max}	0.65, 0.76	0.033, 1.000	0.079, 1.000	0.074, 1.000
No. of measured, independent and observed [I > 2.0σ	35307, 7329, 7293	26697, 6179, 2242	24175, 5560, 2847	22897, 5151, 2851

(I)] reflections				
R_{int}	0.022	0.157	0.119	0.115
$(\sin\theta/\lambda)_{max}$ (Å^{-1})	0.595	0.799	0.797	0.797
Refinement				
$R[F^2 > 2\sigma(F^2)]$, $wR(F^2)$, S	0.028, 0.067, 0.89	0.095, 0.364, 1.08	0.071, 0.238, 1.01	0.067, 0.102, 1.13
No. of reflections	7329	6128	5534	5126
No. of parameters	541	541	445	445
No. of restraints	0	584	584	598
H-atom treatment	H-atom parameters constrained	H-atom parameters constrained	H-atom parameters not refined	H-atom parameters not refined
Dñ$_{max}$, Dñ$_{min}$ (e Å^{-3})	0.88, −0.39	1.19, −1.46	0.73, −0.72	0.74, −0.96

CCDC code	1584753	1584755	1584756
Crystal data			
Temperature (K)	293	293	293
Pressure (GPa)	3.50	4.20	4.50
a, b, c (Å)	14.765 (8), 12.9897 (9), 18.629 (6)	14.652 (7), 12.7677 (9), 18.624 (6)	14.622 (6), 12.6860 (8), 18.613 (6)
β (°)	92.14 (5)	91.96 (5)	92.10 (4)
V (Å^3)	3570 (2)	3482 (2)	3450.3 (19)
D_x (Mg m^{-3})	1.827	1.873	1.891
Radiation type	Synchrotron, l = 0.48590 Å	Synchrotron, l = 0.48590 Å	Synchrotron, l = 0.48590 Å
m (mm^{-1})	1.94	1.99	2.01
Crystal size (mm)	0.04 × 0.02 × 0.02	0.04 × 0.02 × 0.02	0.04 × 0.02 × 0.02
Data collection			
Diffractometer	Pilatus 300K	Pilatus 300K	Pilatus 300K
Radiation source	Diamond Light Source Beamline I19	Diamond Light Source Beamline I19	Diamond Light Source Beamline I19
Monochromator	Double crystal Silicon 111	Double crystal Silicon 111	Double crystal Silicon 111
Absorption correction	Multi-scan *CrysAlis PRO* 1.171.38.41 (Rigaku Oxford Diffraction, 2015) Empirical absorption correction using spherical harmonics,	Multi-scan *CrysAlis PRO* 1.171.38.41 (Rigaku Oxford Diffraction, 2015) Empirical absorption correction using spherical harmonics,	Multi-scan *CrysAlis PRO* 1.171.38.41 (Rigaku Oxford Diffraction, 2015) Empirical absorption correction using spherical harmonics,

	implemented in SCALE3 ABSPACK scaling algorithm.	implemented in SCALE3 ABSPACK scaling algorithm.	implemented in SCALE3 ABSPACK scaling algorithm.
T_{min}, T_{max}	0.3168, 1.000	0.169, 1.000	0.225, 1.000
No. of measured, independent and observed [$I > 2.0s(I)$] reflections	22406, 4883, 2802	19321, 4281, 2817	20918, 4800, 3064
R_{int}	0.106	0.094	0.103
$(\sin q/l)_{max}$ (Å^{-1})	0.797	0.795	0.796
Refinement			
$R[F^2 > 2s(F^2)]$, $wR(F^2)$, S	0.066, 0.092, 1.15	0.059, 0.088, 1.10	0.063, 0.097, 1.11
No. of reflections	4859	4276	4784
No. of parameters	445	445	415
No. of restraints	613	613	542
H-atom treatment	H-atom parameters not refined	H-atom parameters not refined	H-atom parameters not refined
$Dñ_{max}$, $Dñ_{min}$ (e Å^{-3})	0.88, −1.00	0.77, −0.72	0.97, −0.84

Computer programs: Apex2 (Bruker AXS, 2006), *CrysAlis PRO* 1.171.38.41k (Rigaku OD, 2015), *SUPERFLIP* (Palatinus & Chapuis, 2007), *CRYSTALS* (P. W. Betteridge, J. R. Carruthers, R. I. Cooper, K. Prout and D. J. Watkin, *J. Appl. Cryst.*, 2003, **36**, 1487), *CAMERON* (D. J. Watkin, C. K. Prout & L. J. Pearce. Oxford, UK, 1996).

Table S2 Selected structural parameters calculated at the B3LYP-D3/(def2svp + def2tzvp) level in CH_2Cl_2 solution for the $[Cu(P^\wedge P)(N^\wedge N)]^+$ complexes in their electronic ground state S_0 and in their first triplet excited state T_1.

Complex cation	Cu–P distance / Å (Cu1–P1; Cu1–P2)	Cu–N distance / Å (Cu1–N1; Cu1–N2)	P–Cu–P chelating angle / deg	N–Cu–N chelating angle / deg	Angle between P–Cu–P and N–Cu–N planes / deg	N–C–C–N torsion angle /deg
Ground State (S$_0$)						
[Cu(POP)(bpy)]$^+$	2.246; 2.284	2.096; 2.069	113.84	80.09	80.37	14.29
[Cu(xantphos)(bpy)]$^+$	2.269; 2.270	2.104; 2.068	114.40	79.75	86.94	3.23
[Cu(POP)(6,6'-Cl$_2$bpy)]$^+$	2.273; 2.291	2.160; 2.135	113.45	78.17	77.32	21.35
[Cu(xantphos)(6,6'-Cl$_2$bpy)]$^+$	2.271; 2.305	2.141; 2.145	119.27	77.38	86.72	6.76
[Cu(POP)(6-Brbpy)]$^+$	2.259; 2.288	2.110; 2.107	114.88	79.19	79.32	15.50
[Cu(xantphos)(6-Brbpy)]$^{+ a}$	2.280; 2.282	2.123; 2.096	113.74	78.71	87.38	3.30
[Cu(xantphos)(6-Brbpy)]$^{+ b}$	2.249; 2.299	2.112; 2.104	119.25	78.26	87.62	7.60
[Cu(POP)(6,6'-Br$_2$bpy)]$^+$	2.308; 2.281	2.153; 2.152	113.04	77.25	81.45	5.92
[Cu(xantphos)(6,6'-Br$_2$bpy)]$^+$	2.308; 2.282	2.160; 2.159	120.14	77.18	86.44	8.21
Triplet Excited State (T$_1$)						
[Cu(POP)(bpy)]$^+$	2.365; 2.334	1.982; 1.981	102.90	83.46	59.69	2.83
[Cu(xantphos)(bpy)]$^+$	2.350; 2.399	1.997; 1.981	105.92	83.06	57.53	1.99
[Cu(POP)(6,6'-Cl$_2$bpy)]$^+$	2.359; 2.330	2.068; 1.985	104.84	82.11	69.97	2.38
[Cu(xantphos)(6,6'-Cl$_2$bpy)]$^+$	2.360; 2.336	2.095; 1.989	105.69	81.40	77.17	5.42
[Cu(POP)(6-Brbpy)]$^+$	2.407; 2.341	2.000; 1.979	106.06	83.31	68.25	2.89
[Cu(xantphos)(6-Brbpy)]$^+$	2.384; 2.335	2.007; 1.973	106.76	82.58	67.93	3.24
[Cu(POP)(6,6'-Br$_2$bpy)]$^+$	2.381; 2.334	2.112; 1.982	104.69	81.50	73.21	5.38
[Cu(xantphos)(6,6'-Br$_2$bpy)]$^+$	2.370; 2.351	2.123; 1.994	105.43	81.18	78.88	7.20

[a, b] Two different conformations were optimized for the [Cu(xantphos)(6-Brbpy)]$^+$ complex that mainly differ in the orientation of the phenyl rings of the xantphos ligand (Fig. S3). The structure labeled with "*a*" is more similar to the reported X-Ray structure and is depicted in Fig. S3a, whereas the structure labeled with "*b*" corresponds to that displayed in Fig. S3b and appears at slightly lower energies. See the main text for details.
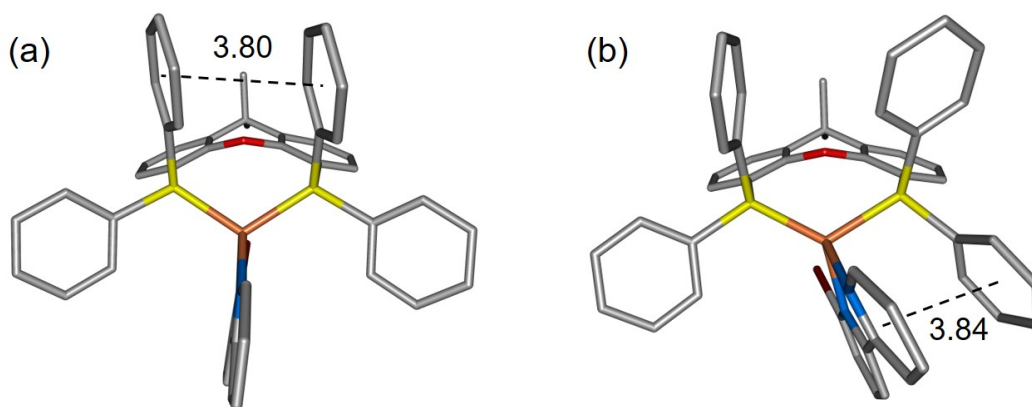
Fig. S4 Minimum-energy conformations calculated at the B3LYP-D3/(def2svp + def2tzvp) level in CH_2Cl_2 solution for [Cu(xantphos)(6-Brbpy)]$^+$. The conformation on the left (a) reproduces closely the X-ray structure reported for this complex. The conformation on the right (b) features a slightly lower energy. Hydrogen atoms are omitted for simplicity.
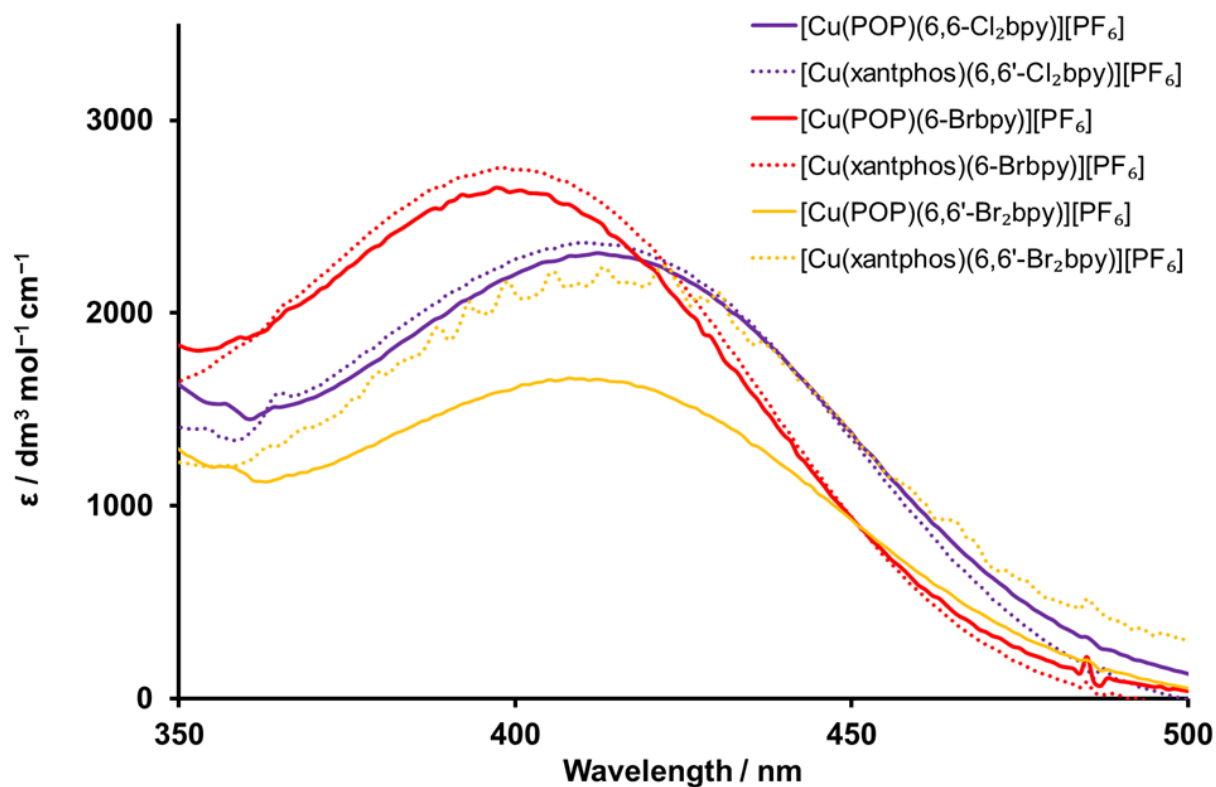

Fig. S5 Zoom into the low-energy MLCT region of the solution absorption spectra of the [Cu(P^P)(bpy)][PF$_6$] complexes (CH_2Cl_2, 2.5×10^{-5} mol dm^{-3}).

Table S3 Vertical excitation energies (E) calculated at the TD-DFT B3LYP/(def2svp+def2tzvp) level for the lowest singlet (S_1) and triplet (T_1) excited states of complexes [Cu(P^P)(N^N)]$^+$ in CH_2Cl_2 solution. $S_0 \rightarrow S_1$ oscillator strengths (f) are given within parentheses. The energy of the T_1 state at its fully optimized TD-DFT geometry is given in the last column.

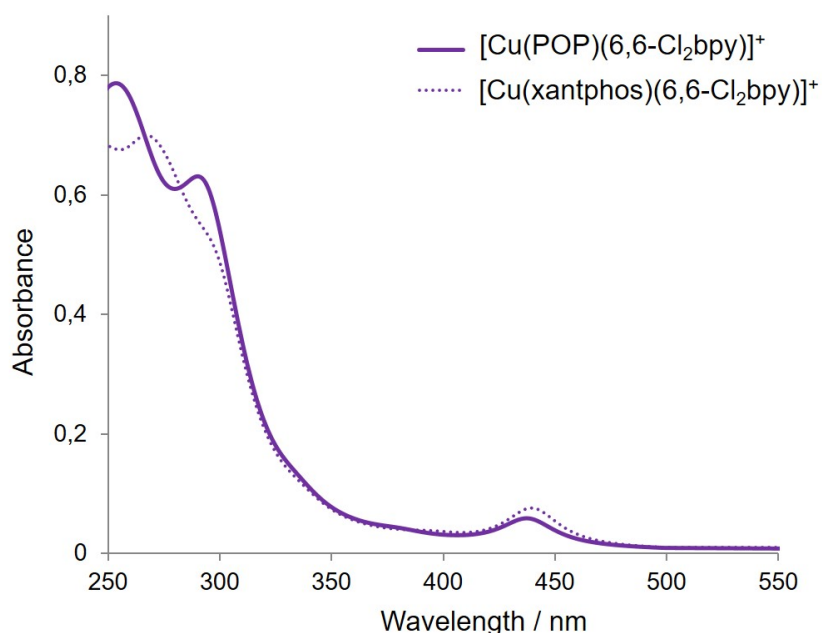| Complex cation	S_1	T_1	T_1 (relaxed)
	E (eV/nm) (f)	E (eV)	E (eV)
[Cu(POP)(bpy)]$^+$	2.800 / 443 (0.08)	2.544	1.220
[Cu(xantphos)(bpy)]$^+$	2.816 / 440 (0.10)	2.569	1.254
[Cu(POP)(6,6'-Cl$_2$bpy)]$^+$	2.618 / 474 (0.06)	2.407	1.423
[Cu(xantphos)(6,6'-Cl$_2$bpy)]$^+$	2.652 / 467 (0.07)	2.418	1.427
[Cu(POP)(6-Brbpy)]$^+$	2.724 / 455 (0.06)	2.486	1.410
[Cu(xantphos)(6-Brbpy)]$^+$	2.730 / 454 (0.07)	2.495	1.423
[Cu(POP)(6,6'-Br$_2$bpy)]$^+$	2.521 / 492 (0.04)	2.355	1.435
[Cu(xantphos)(6,6'-Br$_2$bpy)]$^+$	2.668 / 465 (0.06)	2.447	1.440

Fig. S6 TD-DFT simulations of the absorption spectra calculated at the B3LYP/(6-31G**+LANL2DZ) level of theory in CH_2Cl_2 for [Cu(POP)(6,6'-Cl$_2$bpy)]$^+$ and [Cu(xantphos)(6,6'-Cl$_2$bpy)]$^+$. The spectra were generated by convoluting each electronic transition with a Gaussian function of full-width-at-half-maximum FWHM = 30 nm.
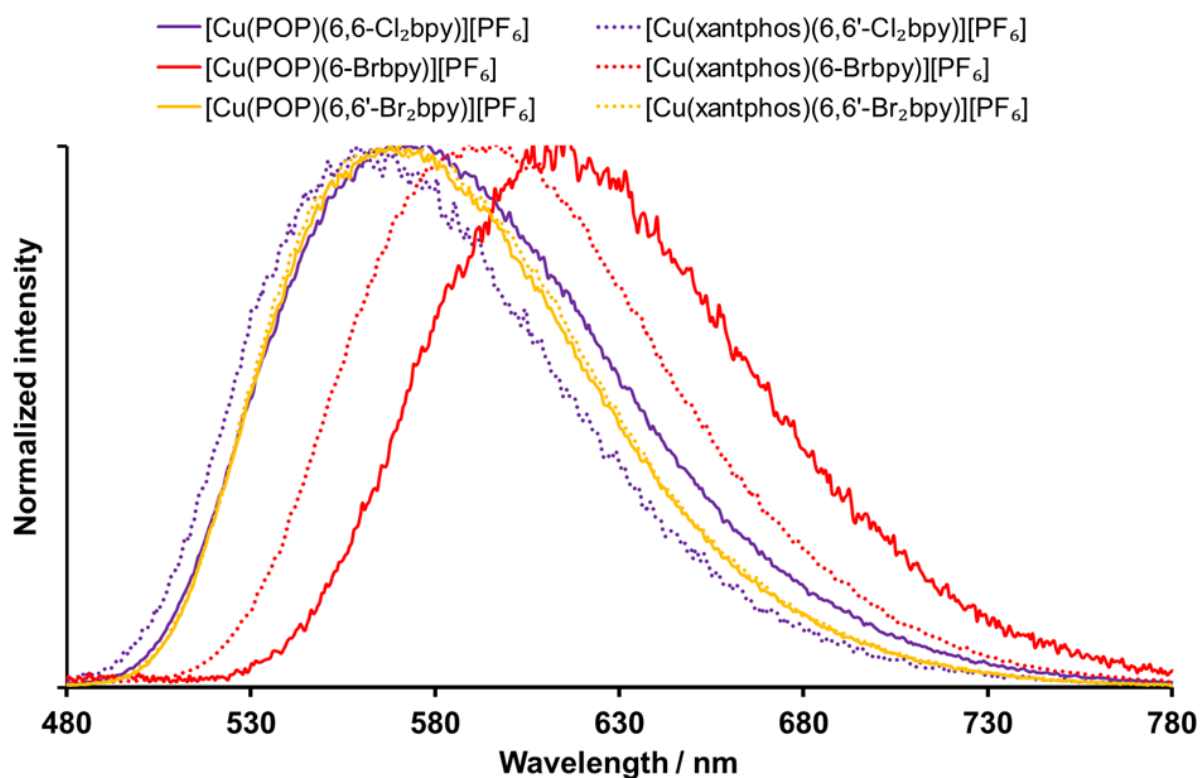
Fig. S7 Normalized emission spectra of the [Cu(P^P)(bpy)][PF$_6$] complexes in a frozen glass of Me-THF (77 K, λ_{exc} = 410 nm).

Fig. S8 Photoluminescence spectra of thin films composed of [Cu(P^P)(6,6'-Cl$_2$bpy)][PF$_6$]:[Emim][PF$_6$] at a 4:1 molar ratio (λ_{exc} = 360 nm).
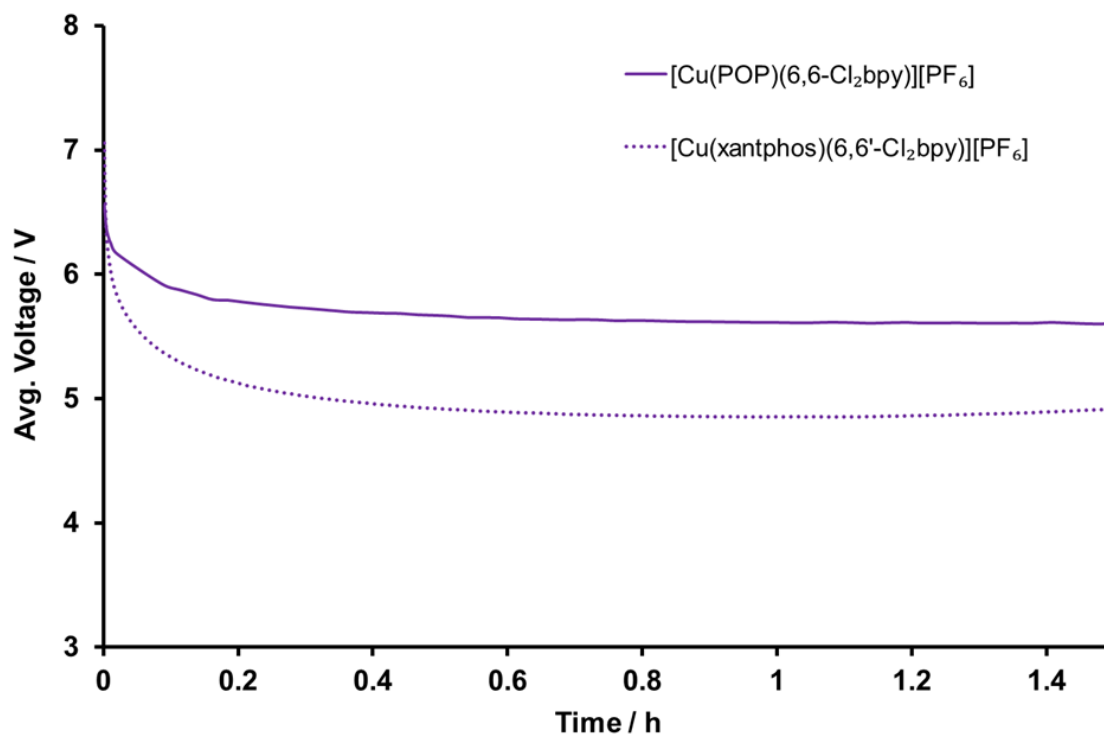
Fig. S9 Average voltage versus time characteristics measured for ITO/PEDOT:PSS/[Cu(P^P)(N^N)][PF$_6$]:[Emim][PF$_6$] 4:1/Al LECs operated at pulsed current (average density current 50 A m^{-2}, 1 kHz, 50% duty cycle, block wave).
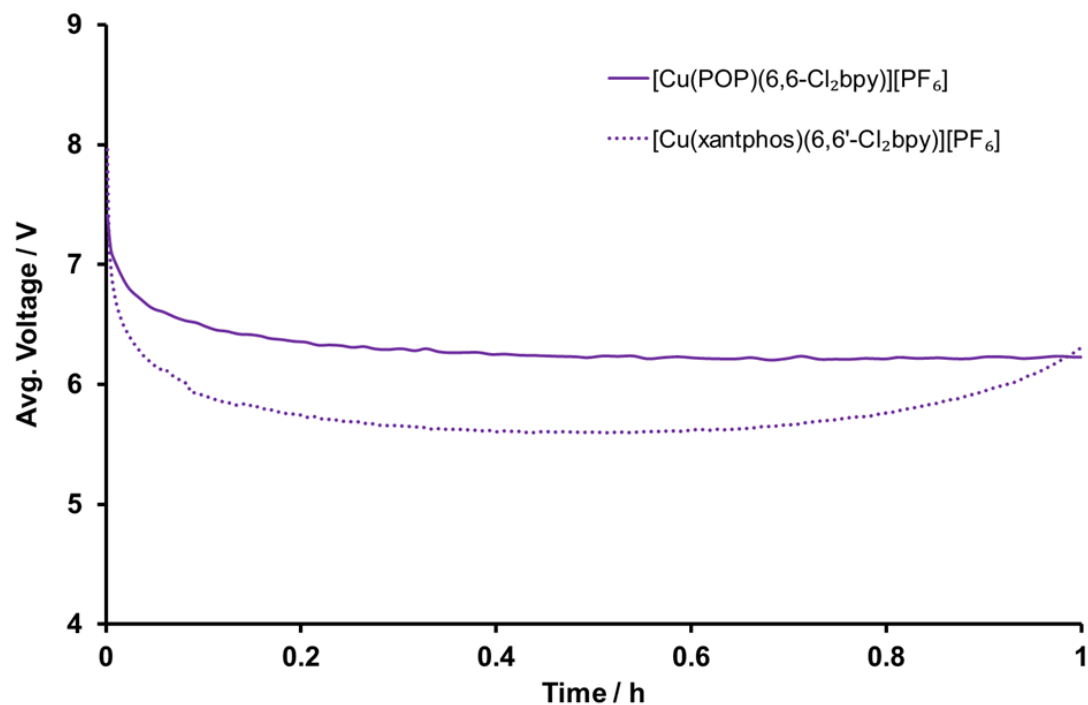

Fig. S10 Average Voltage versus time characteristics measured for ITO/PEDOT:PSS/[Cu(P^P)^N^N)][PF$_6$]:[Emim][PF$_6$] 4:1/Al LECs operated at pulsed current (average density current 100 A m^{-2}, 1 kHz, 50% duty cycle, block wave).